

**EFFECTS OF SYNTHESIS TIME AND CRYSTALLINITY  
ON THE Ni(II) SORPTION PERFORMANCE OF SODIUM  
TITANOSILICATE ION-EXCHANGE COMPOUNDS**

**BY**

**PORNNAPPAN DEESAEN**

**A THESIS SUBMITTED IN PARTIAL FULFILLMENT OF  
THE REQUIRMENTS FOR THE DEGREE OF MASTER OF  
ENGINEERING (ENGINERRING TECHNOLOGY)  
SIRINDHORN INTERNATIONAL INSTITUTE OF TECHNOLOGY  
THAMMASAT UNIVERSITY  
ACADEMIC YEAR 2015**

**EFFECTS OF SYNTHESIS TIME AND CRYSTALLINITY  
ON THE Ni(II) SORPTION PERFORMANCE OF SODIUM  
TITANOSILICATE ION-EXCHANGE COMPOUNDS**

**BY**

**PORNNAPPAN DEESAEN**

**A THESIS SUBMITTED IN PARTIAL FULFILLMENT OF  
THE REQUIRMENTS FOR THE DEGREE OF MASTER OF  
ENGINEERING (ENGINERRING TECHNOLOGY)  
SIRINDHORN INTERNATIONAL INSTITUTE OF TECHNOLOGY  
THAMMASAT UNIVERSITY  
ACADEMIC YEAR 2015**



EFFECTS OF SYNTHESIS TIME AND CRYSTALLINITY ON THE Ni(II)  
SORPTION PERFORMANCE OF SODIUM TITANOSILICATE ION-EXCHANGE  
COMPOUNDS

A Thesis Presented

By

PORNNAPPAN DEESAEN

Submitted to

Sirindhorn International Institute of Technology

Thammasat University

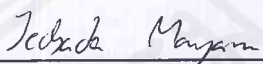
In partial fulfillment of the requirements for the degree of  
MASTER OF ENGINEERING (ENGINEERING TECHNOLOGY)

Approved as to style and content by

Advisor and Chairperson of Thesis Committee


  
\_\_\_\_\_  
(Asst. Prof. Dr. Paiboon Sreearunothai)

Co-Advisor


  
\_\_\_\_\_

(Dr. Jedsada Manyam)

Committee Member and  
Chairperson of Examination Committee

  
\_\_\_\_\_  
(Assoc. Prof. Dr. Pakorn Opaprakasit)

Committee Member

  
\_\_\_\_\_  
(Assoc. Prof. Dr. Ryuichi Egashira)

DECEMBER 2015

## Abstract

### EFFECTS OF SYNTHESIS TIME AND CRYSTALLINITY ON THE Ni(II) SORPTION PERFORMANCE OF SODIUM TITANOSILICATE ION-EXCHANGE COMPOUNDS

by

PORNNAPPAN DEESAEN

Bachelor of Science (Environmental Science), Thammasat University, 2012

Nickel (Ni) is a heavy metal that is commonly employed in the electroplating industries and is of environmental concern due to its toxicity to living organisms. The synthesis time was varied between 1 hour, 6 hours, 1 day and 5 days, and the hydrothermal temperature of 170°C and 200°C, resulting in samples with different crystallinities and sorption performance. The synthesis time of 1 hour was synthesized under room temperature whereas the other samples were synthesized under the hydrothermal reaction. This reaction helps to promote rearrangement of the sorbent structure from amorphous to crystalline structure. It was found that the sample with 6 hours 200°C hydrothermal treatment with semi-crystallinity has the highest Ni sorption capacity of about 108 mg Ni / per g sorbent. The sample that has been hydrothermal for 5 days which has the highest crystallinity, has the lowest Ni adsorption performance of 75 mg Ni / per g sorbent. This is probably due to the rigid crystalline framework which restricts the diffusion of Ni<sup>2+</sup> ions into the structure, and the exchange of the Na<sup>+</sup> with the Ni<sup>2+</sup> ions. The sorption mechanism was found to be predominantly via the ion-exchange mechanism where one Ni<sup>2+</sup> is exchanged with two Na<sup>+</sup> in the adsorbent structure. The developed adsorbents were tested with real electroplating wastewater from local plant containing both Ni and Cr. It can achieve about 84% Ni removal efficiency with the Ni initial concentration of 94 ppm.

**Keywords:** Titanosilicate, Nickel, Adsorption, Natisite



## Acknowledgements

This thesis would not have been possible without the help and support of many people. I would like to thank all of those people who have made this experience unforgettable.

Firstly, I express the deepest appreciation to my beloved advisor, Asst. Prof. Dr. Paiboon Sreearunothai, for the continual support, guidance and advice provided throughout the research. His dedication to the research inspired me to take my work to new levels. Moreover, he has given me the friendship and chance to participate in a variety of valuable experiences. His recommendations always help me in all the time of research and writing of this thesis. Our discussion has made me improved my research skills and ready for further study.

Secondly, I also would like to acknowledge and pay my sincere thanks to my co-advisor, Dr. Jedsada Manyam from NANOTEC, for his time, comment and his valuable advice throughout my study. I would like to thank him for his conveniently providing in using some equipment at his place. Thirdly, I would like to acknowledge and pay my special thanks to Assoc. Prof. Dr. Pakorn Opaprakasit. His expertise in FTIR analysis has guided me to comprehend the characterization of the sodium titanate before and after adsorption.

In addition, I would also like to express my respect and thank to Assoc. Prof. Dr. Ryuichi Egashira from TIT, for their assistance and suggestions throughout my project. Finally, I would like to say thank to TAIST- Tokyo Tech scholarship for giving me this opportunity. Without the guidance of my advisor and committee members, this thesis would never have been completed.

## Nomenclatures

$C_e$	Equilibrium metal ion concentration (mg/l)
$\Delta$	Hydrothermal reaction
BET	Brunauer-Emmett-Teller
$C_0$	Initial metal ion concentration (mg/l),
EDS	Energy Dispersive X-ray Spectrometer
EPA	Environmental Protection Agency
FTIR	Fourier Transform Infrared Spectroscopy
ICP-OES	Inductively Couple Plasma-Optical Emission Spectrometer
$K_L$	Langmuir constant (l/mg)
$Q_e$	Amount of metal ions adsorbed on adsorbent at equilibrium (mg/g)
$Q_{max}$	Maximum adsorption capacity (mg/g)
R	Removal efficiency (%)
RT	Room temperature
SEM	Scanning Electron Microscopy
TEOS	Tetraethyl orthosilicate
TIPO	Titanium (IV) isopropoxide
TLV	Threshold Limit Value
TSi	Sodium titanosilicate
XRD	X-ray Diffraction

## Table of Contents

Chapter	Title	Page
	Signature Page	i
	Abstract	ii
	Acknowledgements	iv
	Nomenclatures	v
	Table of Contents	vi
	List of Tables	ix
	List of Figures	x
1	Introduction	1
	1.1 Concepts and significance	1
	1.2 Objectives	2
	1.3 Scope of the study	3
2	Literature review	4
	2.1 Properties of Nickel	4
	2.1.1 Environmental effects of nickel	5
	2.1.2 Effects on human health	6
	2.1.3 Nickel in the electroplating industry	6
	2.1.4 Nickel removal techniques	7
	2.2 The framework sodium titanate under this study	11
	2.2.1 Characteristics of the sodium titanate	14
	2.2.2 Ion exchange mechanism of the sodium titanate	16
3	Methodology	18
	3.1 Sample preparation	18



3.2	The preparation of Ni(OH) <sub>2</sub>	20
3.3	Sample characterizations	21
3.3.1	Sample structure	21
3.3.2	Samples morphology	22
3.3.3	Sample pore size	22
3.3.4	Sample functional group	22
3.3.5	Heavy metal concentration analysis	22
3.4	Batch sorption experiment	23
3.4.1	Sorption capacity	23
3.4.2	Real wastewater	23
3.4.3	Regeneration and reusability of the selected adsorbents	23
4	Results and discussion	25
4.1	Characterization of samples before adsorption	25
4.1.1	Structural characterization	25
4.1.2	Morphology characterization	27
4.2	Adsorption isotherm	30
4.2.1	Sorption Capacity	30
4.3	Ion exchange mechanism between Ni <sup>2+</sup> in solution Na <sup>+</sup> on adsorbents	35
4.4	Surface area and pore size of the selected adsorbents	38
4.5	Characterization of selected adsorbent after Ni adsorption	39
4.5.1	Structural characterization	39
4.5.2	Morphology characterization	40
4.5.3	Elemental composition characterization	43
4.5.4	Functional group characterization	44
4.6	Regeneration and reusability of the selected adsorbents	46
4.6.1	Removal efficiency of selected adsorbent after regeneration	47

4.6.2	Characteristics of selected adsorbents after regeneration and reusability	48
4.7	The real wastewater adsorption of the selected adsorbents	53
5	Conclusions and Recommendation	55
5.1	Conclusions	55
5.2	Recommendation and future work	57
	References	58

## List of Tables

Tables	Page	
2.1	General chemical properties of Ni [31]	4
2.2	Quality standards and effluent from industrial estates [37]	5
2.3	Concentrations of Nickel in plating baths [32]	7
2.4	Adsorbents is used for Ni removal from wastewaters [41].	9
2.5	Chemical formula and structure fragments of each crystalline titanosilicate phases: $T_p$ is five-coordinated $Ti^{4+}$ , $T_o$ is six-coordinated $Ti^{4+}$ , $Q^n$ is $SiO_4$ tetrahedron connected with $n$ adjacent $SiO_4$ tetrahedra [25]	12
2.6	Surface area and pore volume of titanosilicate [62]	16
2.7	Surface properties of mesoporous titanosilicate [63]	16
3.1	List of chemicals that were used in this study	18
4.1	Langmuir isotherms of synthesis adsorbents is compared with resin (commercial grade)	33
4.2	Langmuir parameters of the selected adsorbents	35
4.3	Mole ratio of $Na^+$ in solution and $Ni^{2+}$ onto each selected adsorbent: (A) TSi-5d $\Delta$ 170°C, (B) TSi-1d $\Delta$ 170°C, (C) TSi-6h $\Delta$ 200°C, and (D) TSi-1h-RT (M.W. of Ni = 58.69 g/mole, M.W. of Na = 22.99 g/mole)	36
4.4	BET results of selected adsorbents from BJH model	38
4.5	Elements (% weight) on surface of the selected adsorbent (Bf : Before Ni adsorption, and Af : After Ni adsorption)	43

## List of Figures

Figures	Page	
2.1	Precipitation of metal salts at various pH values [32]	8
2.2	Structure of sodium titanosilicate in polyhedral representation as viewed down [59]	11
2.3	Crystal structures of paranatisite (A) and natisite (B) [24]	13
2.4	XRD patterns (left) and FTIR spectra (right) of natisite or sodium titanosilicate [60]	14
2.5	SEM images of natisite: natisite k-silica (left) and natisite n-silica (right) [61]	15
3.1	Flow chart of the synthesis conditions	19
3.2	Hydrothermal Teflon-lined pressure vessel (left) and the mixture of precursor reagents in the plastic beaker (right)	20
3.3	Ni (OH) <sub>2</sub> (A) and NiSO <sub>4</sub> powder (B)	21
4.1	XRD pattern of each condition of synthetic adsorbents before Ni adsorption: (A) TSi-5dΔ170°C, (B) TSi-1dΔ170°C, (C) TSi-6hΔ200°C, (D) TSi-6hΔ170°C, and (E) TSi-1h-RT	26
4.2	SEM images of synthesis adsorbents in each condition before Ni adsorption: (A) TSi-5dΔ170°C, (B) TSi-1dΔ170°C, (C) TSi-6hΔ200°C, (D) TSi-6hΔ170°C, and (E) TSi-1h-RT	28
4.3	FTIR spectra of synthesis adsorbents: (A) TSi-5dΔ170°C, (B) TSi-1dΔ170°C, (C) TSi-6hΔ200°C, (D) TSi-6hΔ170°C, and (E) TSi-1h-RT	30
4.4	Fitting of Langmuir model (Eq.4.1) to plot evaluate maximum Ni adsorption capacity: (A) TSi-5dΔ170°C, (B) TSi-1dΔ170°C, (C) TSi-6hΔ200°C, (D) TSi-6hΔ170°C, (E) TSi-1h-RT, and (F) Resin	32
4.5	Experimental data of the selected adsorbents fitted with the Langmuir model.	34

4.6	XRD patterns of the selected adsorbents before and after adsorption: (A) TSi-5d $\Delta$ 170 $^{\circ}$ C, (B) TSi-1d $\Delta$ 170 $^{\circ}$ C, (C) TSi-6h $\Delta$ 200 $^{\circ}$ C, and (D) TSi-1h-RT	40
4.7	SEM images of the selected adsorbents before (left) and after (right) adsorption. From top to bottom: TSi-5d $\Delta$ 170 $^{\circ}$ C, TSi-1d $\Delta$ 170 $^{\circ}$ C, TSi-6h $\Delta$ 200 $^{\circ}$ C, and TSi-1h-RT	42
4.8	FTIR spectra of the selected adsorbents before and after Ni adsorption: (A) TSi-5d $\Delta$ 170 $^{\circ}$ C, (B) TSi-1d $\Delta$ 170 $^{\circ}$ C, (C) TSi-6h $\Delta$ 200 $^{\circ}$ C, and D) TSi-1h-RT. The arrows are at 888, 843, 725, and 624 $\text{cm}^{-1}$ correspond to peak positions in the pristine crystalline samples shown earlier, while those at 1252 and 1118 $\text{cm}^{-1}$ corresponded to that of the sulfate group of the NiSO <sub>4</sub> solution used.	45
4.9	FTIR spectra of selected adsorbents after Ni adsorption are compared with the spectra of the NiSO <sub>4</sub> powder.	46
4.10	Removal efficiency of Ni of select adsorbents in three cycles	48
4.11	SEM images of selected adsorbents after regeneration and reusability	49
4.12	FTIR spectra of selected adsorbents after reusability	51
4.13	FTIR of selected adsorbents after reusability in second cycle are compared with the homemade NiOH and the NiSO <sub>4</sub> powder.	52
4.14	Ni removal efficiency of the selected adsorbent is compared between the real wastewater and the synthetic Ni solution	54

# Chapter 1

## Introduction

### 1.1 Concepts and significance

Heavy metal contamination in water is part of an environmental problem in many countries. Various heavy metals are utilized in many industries such as metal plating industries [1], batteries [2], pesticides [3] and paper industries [4]. Well-known of heavy metals are chromium, cobalt, nickel, copper, zinc, arsenic, selenium, silver, cadmium, antimony, mercury, thallium and lead [5, 6]. They are not biodegradable and can lead to accumulation in sediment or living organisms.

Nickel (Ni) is one of heavy metals that may be found in the mining industries [7], electroplating [8], and battery manufacturing [9]. Accumulation of Ni (II) can affect living organism. If nickel is taken into the body either by inhalation or ingestion, it may lead to lung cancer or induce cardiovascular diseases [10]. The maximum amount of nickel in drinking water as regulated by the World Health Organization (WHO) is 0.1 mg/l or 0.1 ppm[11].

Numerous methods for heavy metal removal have been investigated such as chemical precipitation, ion-exchange [12], membrane filtration, solvent extraction and electrolysis, reverse osmosis [13], biological treatment [14], and adsorption[15]. Among them, adsorption technique is a simple technique for wastewater treatment and also has high removal efficiency. Previous studies have included the usage of inorganic and organic adsorbents such as zeolite [16, 17], kaolinite, chitosan, orange peel [18] and titanosilicate compounds [5, 19]. Amongst these, titanosilicate compounds have been reported to have high that is an effective material for heavy metals removal.

The titanosilicate compounds are one of the inorganic adsorbents [19] which consists of network of Ti octahedra and Si tetrahedra. Titanosilicate compounds can be synthesized by several methods such as hydrothermal [20, 21], and sol-gel reactions [19]. The hydrothermal reaction has been recognized as an effective method because of

its high ability to produce the crystalline structure [22]. Several researches [23-25] normally employ long hydrothermal time in order to create the crystalline structure of the titanosilicate. The suitable structures of the titanosilicate compounds depend on the types of the applications. The high crystalline structure may be necessary for applications in catalysis where precise geometry is important for the catalyst reaction to take place. Several researches [19, 21, 26] have shown various types of titanosilicate compounds to have high performance for removing radioactive nuclides such as cesium and strontium. However, the structure with the high crystallinity may not always have the highest adsorption performance, which depends rather on the ion-exchange ability of the material. The major mechanism of the titanosilicate compound in adsorbing radioactive nuclides was shown to be through the ion-exchange mechanism [27, 28].

This work studies the utilization of one of the titanosilicate compounds known as natisite for use in removal of Ni(II) from wastewater. It also studies the effects of synthesis conditions on the Ni removal performance. The various synthesis times plays an important role in determining the crystallinity and the Ni sorption performance of the synthesized adsorbents.

## **1.2 Objectives**

This study aims to investigate the use of titanosilicate in Nickel removal from wastewater. Titanosilicate as adsorbents were prepared by different methods. The specific objectives of this study were as follows:

- 1.2.1 To investigate the appropriate structure of the sodium titanosilicate for Ni removal
- 1.2.2 To investigate the Ni adsorption performance of the titanosilicate in batch experiment
- 1.2.3 To study the ion exchange mechanism between the sodium in the synthesized adsorbents and nickel ions in the solution
- 1.2.4 To study the regeneration and reusability of the synthesized adsorbents

### **1.3 Scope of the study**

The study mainly focuses on the Ni adsorption performance of the synthetic sodium titanate at various hydrothermal time and temperature, which is used as an adsorbent. The characteristics of the adsorbents (structure, morphology, functional group, and surface area) before and after Ni adsorption were analyzed in order to investigate the characteristics changed. The Ni adsorption onto the adsorbent was explained by the ion-exchange properties of the sodium titanate. The real wastewater was obtained from local electroplating industry, and the simulated nickel solution was prepared using  $\text{NiSO}_4 \cdot 6\text{H}_2\text{O}$ . The regeneration and reusability of the adsorbents was studied using 0.5M NaOH. The morphology and functional group of the adsorbents after regeneration and reuse were also characterized in order to observe the characteristics changed.



## Chapter 2

### Literature review

In this chapter, physical and chemical properties of Ni are provided. The effect of Ni to the environment and effect on human health are given. The Ni removal methods are discussed, especially adsorption and ion exchange methods. Thus, the properties of material, which is used as an adsorbent, are presented.

#### 2.1 Properties of Nickel

Nickel (Ni) is one of heavy metal that is a well-known toxic material. Physical properties of Ni as a solid are a silvery white metal, hard, and conduct electricity [29], whereas compounds of nickel are blue or green. Chemical properties of Ni are very slowly react with oxygen in air at ambient temperature [30], and highly resistant to corrosion. General chemical properties of Ni are demonstrated in table 2.1.

Table 2.1 General chemical properties of Ni [31]

Physical and chemical properties	Values
Molar mass	58.81 g/mole
Density	8.9 g/cm <sup>-3</sup> at 20°C
Melting point	1453 °C
Boiling point	2913°C
Ionic radius	0.069 nm
Vander Waals radius	0.124 nm

In the environment, Ni is found in low-level due to naturally occur from the earth's crust and it was also combined with oxygen or sulfur in the air [29]. This metal is widely used in the electroplating [32, 33], batteries [34], and catalysts [35] processes. Nickel compounds can be increasingly emitted into the environment by the polluted discharge of industries. It also distributes in the air, water, soil, and food [36] that resulting in Ni contaminated in the environment and pass into the food chain. Effects on

human health of nickel can occur by various routes of exposure such as inhalation, oral, and dermal exposure of nickel [29].

### 2.1.1 Environmental effects of nickel

Nickel in the environment is mostly released from manufacturing and processing facilities in industrials. Therefore, Ni is transported into the air, water, and soil. Nickel compound is released to the air in aerosols or suspended particles form. It normally occurs from windblown dust, municipal incinerators, and burning fuel oil. Nickel is mostly found in wastewater from industries. Nickel can pass into the aquatic ecosystem and also enter into human [29].

In Thailand, there are many industrial estates in around Bangkok. The wastewater from the industrial estates is mostly contaminated with heavy metals, and then it is directly released into the water. Pollution Control Department, Thailand [37] that limits the water quality index of the industrial wastewater, as shown in table 2.2. The limitation of Ni is should not more than 1 mg Ni/l.

Table 2.2 Quality standards and effluent from industrial estates [37]

Water quality index	Standard values	Method for examination
Heavy metals		
1. Zinc (Zn)	Not more than 5.0 mg/l	
2. Chromium (Hexavalent)	Not more than 0.25 mg/l	Atomic Absorption
3. Chromium (Trivalent)	Less than 0.75 mg/l	Spectrophotometry of
4. Copper (Cu)	Not more than 2.0 mg/l	Direct Aspiration or
5. Cadmium (Cd)	Not more than 0.03 mg/l	Plasma Emission
6. Barium (Ba)	Not more than 1.0 mg/l	Spectroscopy of
7. Lead (Pb)	Not more than 0.2 mg/l	Inductively Coupled
8. Nickel (Ni)	Not more than 1.0 mg/l	Plasma: ICP.
9. Manganese (Mn)	Not more than 5.0 mg/l	
10. Arsenic (As)	Not more than 0.25 mg/l	Hydride Generation

11. Selenium (Se)	Not more than 0.02 mg/l	Atomic Absorption Spectrophotometry type or Plasma Emission Spectroscopy of Inductively Coupled Plasma: ICP.
12. Mercury (Hg)	Not more than 0.005 mg/l	Atomic Absorption Cold Vapor Technique

### 2.1.2 Effects on human health

Effect on human health, it can be provided into the acute, sub-chronic and chronic effects. Those effects are depended on route of exposure and concentrations of Ni that pass into human body [38]. For example, effect of nickel is reduced lung function, and damage to nasal cavity [29]. Acute effect of nickel or short term exposure is disrupting irritation and pneumonitis. On the other hand, long term exposure or chronic effect of nickel has been connected with increased risk of lung cancer, cardiovascular disease, neurological deficits, and developmental deficits in childhood, and high blood pressure. Therefore, The National Institute for Occupational Safety and Health [39] determine the limitation of nickel for worker who directly expose with nickel, Threshold Limit Value (TLV) for inhalation fraction is 1.5 mg/m<sup>3</sup>. Nickel is classified to be carcinogen category I [40], which is substance to increase cancer or induce benign and malignant tumours in human body. Additionally, nickel has been identified as a toxin that severely damages reproductive health and can lead to infertility, miscarriage, birth defects, and nervous system defects.

### 2.1.3 Nickel in the electroplating industry

Nickel is widely used in the electroplating industry [36]. For example, an electroplating industry of Hong Kong [32] that has various plating type such as copper, nickel, chromium, zinc, gold, silver, tin, lead, and aluminium anodizing. Table 2.3 only

shows the concentration of Ni, which is used in Ni plating process. Additionally, the remaining of Ni concentration may be contaminated in the discharge wastewater.

Table 2.3 Concentrations of Nickel in plating baths [32]

Type of plating	Plating bath composition	
Nickel (Ni <sup>2+</sup> )	Nickel sulphate	240-300 g/l
	Nickel chloride	45-60 g/l
	Boric acid	30-40 g/l

#### 2.1.4 Nickel removal techniques

The various techniques are used for Ni removal from wastewater such as chemical precipitation, ion-flotation, ion-exchange, membrane filtration, adsorption, and electrochemical treatment [5]. Nevertheless, the general methods are chemical precipitation, ion-exchange, and adsorption, which are discussed in next section.

##### 2.1.4.1 Chemical precipitation

Nickel is precipitated by raising the pH to basic conditions, typically pH9-10 that seen in figure 2.1 [32]. It is called chemical precipitation, and nickel is transformed into the highly insoluble Ni hydroxide, Ni(OH)<sub>2</sub>. The precipitation was performed at elevated temperature, 65-95 °C, when Ni(OH)<sub>2</sub> could be obtained by super saturation controlled precipitation[41].

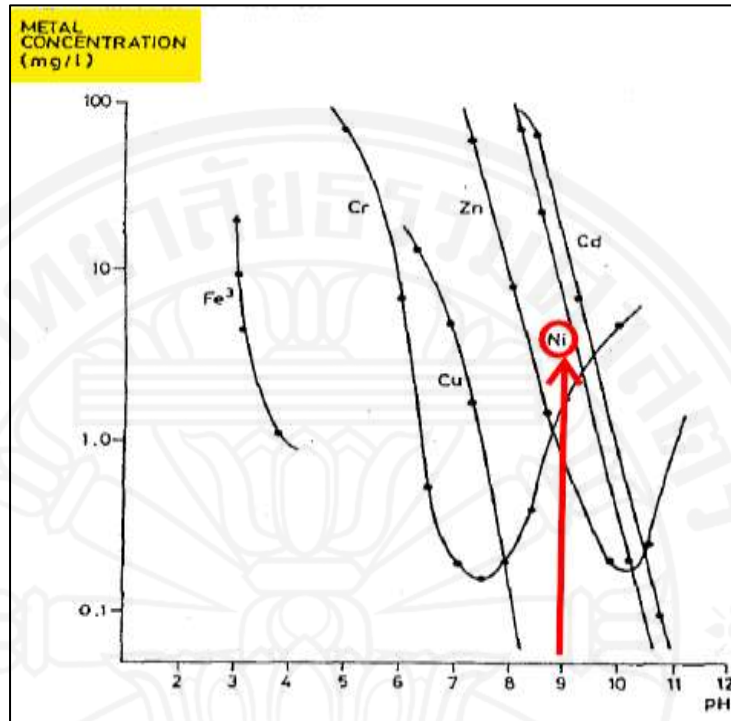
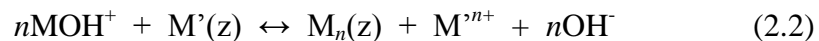


Figure 2.1 Precipitation of metal salts at various pH values [32]

#### 2.1.4.2 Ion exchange

Ion exchange is one of predominant applied treatments for heavy metals removal. By using this technique, undesirable ions are replaced by other ions which are harmless to the environment. Moreover, this technique may be combination with other techniques for increasing the removal efficiency [41]. In case, ion exchange is combined with adsorption technique. The exchange process is related to the metal ions on adsorbent due to its exchange between the adsorbent surface and divalent metal in nickel solution [42]. A useful example of ion exchange mechanism of zeolite framework, which is close to the adsorbent in this study, is the exchangeable between the metal ion in zeolite framework ( $M'(z)$ ) and the hydrolyzed divalent metal ion ( $M^{2+}$ ) in aqueous solution ( $MOH^+$ ). The reaction is following this equation [42] :



### 2.1.4.3 Adsorption

Adsorption method is widely used for heavy metals removal due to its flexibility, reversible process, and easy operation to remove nickel or other metal from wastewater [43]. Adsorption method is a mass transfer process, by which a compound is transferred and accumulated at the interface between two phases (liquid–solid, gas–solid). The substance binds to the surface of the solid phase through physico/chemical interactions and becomes the adsorbate, while the solid on which adsorption takes place is called the adsorbent [41]. Several studies investigate the adsorption capacity of Ni have been carried out on the various adsorbents, as shown in table 2.4.

Table 2.4 Adsorbents is used for Ni removal from wastewaters [41].

Adsorbents	Adsorption capacity (mg/g)	References
Synthetic zeolite	60	[44]
Natural kaolinite	2	[45]
MWCHTs	49	[46]
MWCNTs/iron oxide magnetic composites	9	[47]
<i>Escherichia coli</i> biofilm	15	[48]
Chitosan coated PVC beads	120	[49]
Apricot stone	27	[50]
Tea factory waste	15	[51]
Protonated rice bran	102	[52]
Orange peel	158	[18]

Adsorption model is used to determine adsorption characteristics from the adsorption parameters [53]. Langmuir sorption isotherm is one of the adsorption models, which is assumed as monolayer process and homogeneous adsorption surface. Langmuir

parameters describe the maximum adsorption capacity and show the affinity to adsorb. The Langmuir isotherm can be expressed by following equation [53]:

$$Q_e = \frac{Q_{max} K_L C_e}{1 + K_L C_e} \quad (2.1)$$

where  $Q_e$  is the amount of metal ions adsorbed on adsorbent at equilibrium (mg/g),  $Q_{max}$  is the maximum adsorption capacity (mg/g),  $K_L$  is the Langmuir constant (l/mg), and  $C_e$  is the equilibrium aqueous metal ions concentration (mg/l). The values of  $Q_{max}$  (mg/g) and  $K_L$  (l/mg) can be determined from the linear plot of  $C_e/Q_e$  versus  $C_e$ .

From table 2.4, the inorganic materials (synthetic zeolite, natural kaolinite, MWCHTs, and MWCNTs/iron oxide magnetic composites) have low Ni adsorption capacity. Therefore, the sodium titanosilicate, which is one of inorganic material, is studied in this study.

From the several researches show the adsorption capacity of the titanosilicate framework for heavy metals removal. The Engelhard titanosilicate (ETS) is one of the titanosilicate frameworks. Huimin Liu [54] studied that the adsorption performance of ETS-1 and ETS-2 in the removal of monovalent  $Ag^+$ , divalent cations ( $Cu^{2+}$ ,  $Sr^{2+}$ ), and trivalent cations ( $Cr^{3+}$ ,  $Y^{3+}$ ,  $Fe^{3+}$ ). The ETS-1 and ETS-2 had the highest adsorption performance for monovalent  $Ag^+$  at 3.45 mmol/g and 3.64 mmol/g, respectively. For the divalent cations, the adsorption capacities were about 1.41-1.52 mmol/g. Jong Hun Choi [55] investigated that the applied of the nano-sized ETS-10 to the removal of  $Cu^{2+}$ ,  $Co^{2+}$ ,  $Mn^{2+}$ , and  $Zn^{2+}$ . The adsorption capacities of  $Cu^{2+}$ ,  $Mn^{2+}$ ,  $Zn^{2+}$ , and  $Co^{2+}$  were 1.55, 1.3, 0.98, and 0.91 mmol/g, respectively, which are calculated by the Langmuir isotherm. For example, the adsorption capacities of strontium, mercury, and cobalt is 1.95 mmol/g [19], 0.00043 mmol/g [56], and 58 mg/g [57], respectively. Therefore, the adsorption capacities of the divalent cations may be about 1.4 – 1.5 mmol/g.

## 2.2 The framework sodium titanate under this study

Sodium titanate is an adsorbent that is used in this study. This adsorbent has many applications such as in catalyst, ion exchange, separation processes. The sodium titanate is one of inorganic materials. It is part of the titanate framework consisting network of interconnected  $\text{TiO}_5$  square pyramids and  $\text{SiO}_4$  tetrahedra with  $\text{Na}^+$  ions interstitial cavities [58]. Figure 2.2 shows the sodium titanate structure that has cavity site to enclose the sodium ions, and its bonding with two water molecules [59].

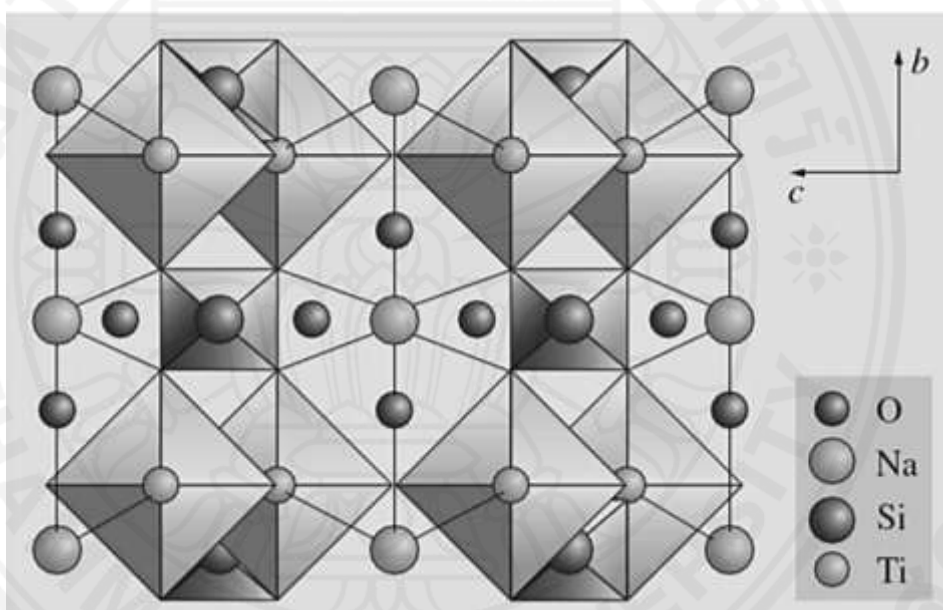
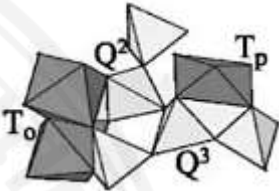
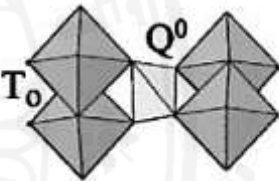
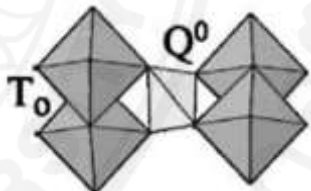
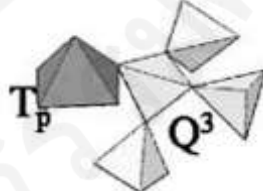
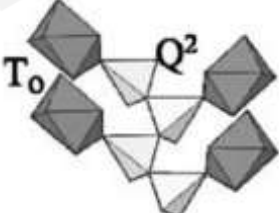


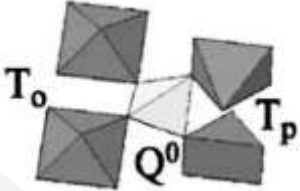
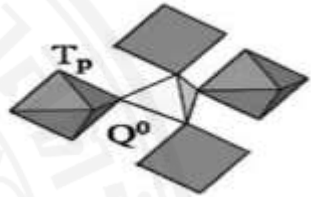
Figure 2.2 Structure of sodium titanate in polyhedral representation as viewed down [59]

Crystalline phase of the sodium titanate is obtained from hydrothermal reaction and molecular ratios of  $\text{Ti}/\text{Si}$ , as shown in table 2.5 [25]. The last row (highlighted row) of this table is chemical formula and structure of natisite, which is used in this study. The ratio  $\text{Na}_2\text{O}/\text{TiO}_2$  is vital for the type of incipient  $\text{SiO}_4\text{-TiO}_n$  clustering and thus for the formation of crystalline titanate phases of desired framework topology [25].



Table 2.5 Chemical formula and structure fragments of each crystalline titanosilicate phases:  $T_p$  is five-coordinated  $Ti^{4+}$ ,  $T_o$  is six-coordinated  $Ti^{4+}$ ,  $Q^n$  is  $SiO_4$  tetrahedron connected with  $n$  adjacent  $SiO_4$  tetrahedra [25]

Name	Chemical formula	Ti/Si	Structural fragment
<b>ETS-4</b> (microporous)	$H_2Ti_4Si_{12}O_{38}(TiO)Na_8 \cdot 8.5H_2O$	0.42	
<b>GTS-1</b> (microporous)	$HM_3Ti_4O_4(SiO_4)_3 \cdot 4H_2O$ (M=Na)	1	
<b>Sitinakite</b> (microporous)	$Na_2Ti_2O_3SiO_4 \cdot 2H_2O$	2	
<b>AM-1 (layered)</b>	$Na_4Ti_2Si_8O_{22} \cdot 4H_2O$	0.25	
<b>AM-4(layered)</b>	$Na_3(Na,H)Ti_2O_2(Si_2O_6) \cdot 2H_2O$	0.5	

Name	Chemical formula	Ti/Si	Structural fragment
<b>Paranatisite (dense)</b>	$\text{Na}_8\text{Ti}_{3.5}\text{O}_2(\text{OH})_2(\text{SiO}_4)_4$	0.88	
<b>Natisite (dense)</b>	$\text{Na}_2(\text{TiO})(\text{SiO}_4)$	1	

Furthermore, the synthesis time may be leads to crystal structure: paranatisite and natisite. Due to the hydrothermal reaction at 200 °C of 24 hours and 144 hours affect the different structure, as show in figure 2.3 [24].

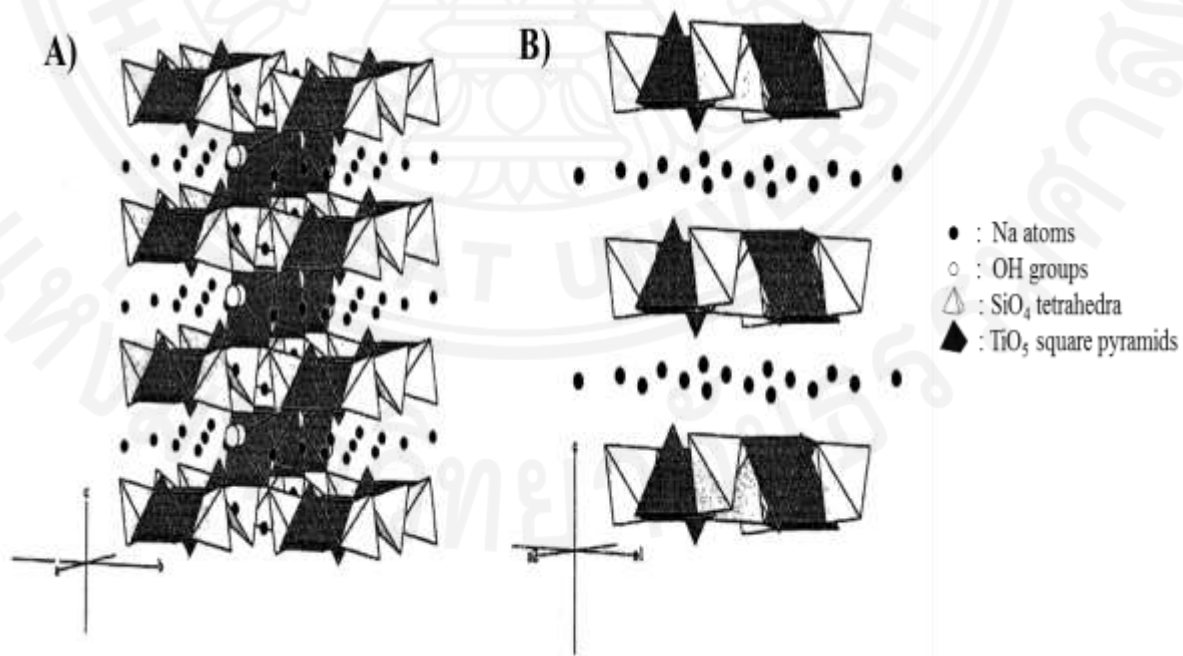


Figure 2.3 Crystal structures of paranatisite (A) and natisite (B) [24]

### 2.2.1 Characteristics of the sodium titanate

The structure of the sodium titanate has been investigated by X-Ray Diffractometry (XRD), whereas the functional group is observed by FTIR adsorption as shown in figure 2.4. The structure of the sodium titanate may be changed when the synthesis temperature also changed. These changes affect the phase transformation as well, it is proven by IR adsorption. Gow-Weng Peng [60] explained that the hydrothermal reaction produces the natsite phase due to its appearance of the predominant IR peak at 725 and 624  $\text{cm}^{-1}$ , and these peaks change as follows by the synthesis temperature. Moreover, the hydrothermal reaction results in a high crystalline structure, which is shown by XRD. In this study, the synthetic method of sodium titanate is close to the previous synthetic method from this paper [60]. So the results of this study are nearly the same as well, as shown in Figure 2.4(A).

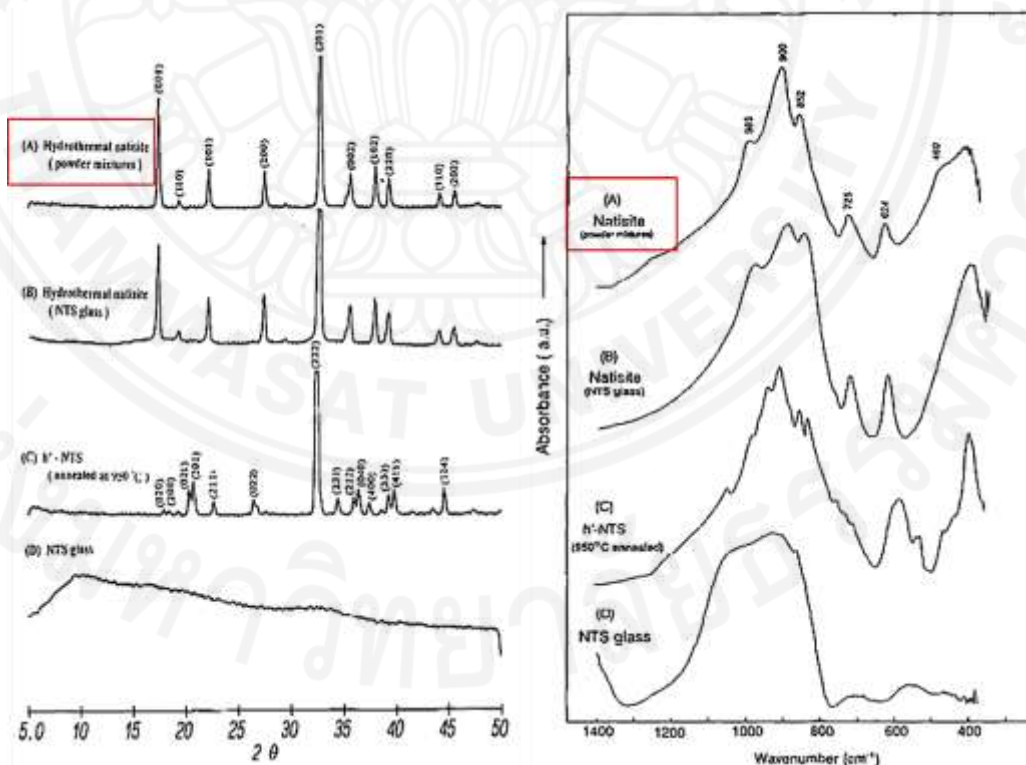


Figure 2.4 XRD patterns (left) and FTIR spectra (right) of natsite or sodium titanate [60]

The morphology of this materials has been investigated by Scanning Electron Microscopy (SEM) in order to evaluation of the heterogeneous or homogeneous surface morphology. The morphology is modified following the experiment conditions from the previous reserch [23]. N. Ismail [61] showed the different morphology of natisite when source of silica is changed. Nevertheless, the morphology of natisite shows the cuboids shape is observed by SEM that the crystalline structure can be confirmed, as shown in figure 2.5.

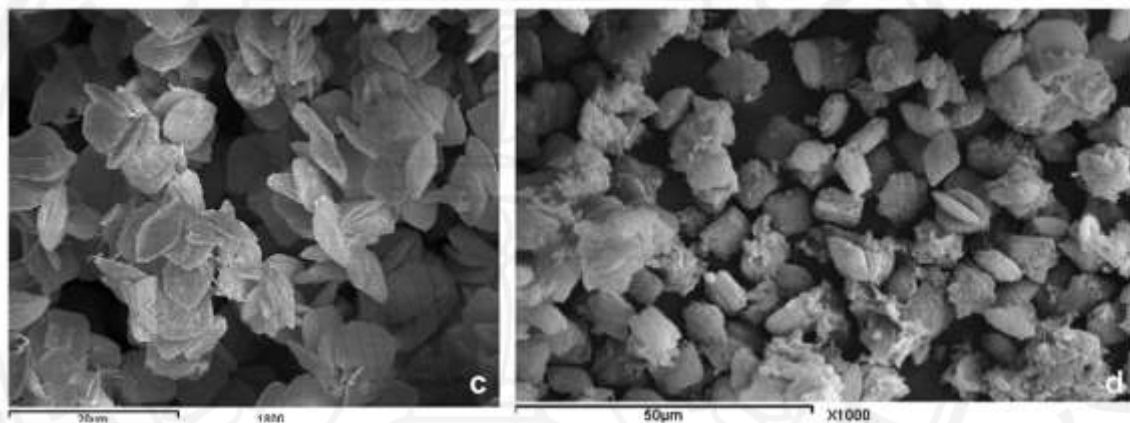


Figure 2.5 SEM images of natisite: natisite k-silica (left) and natisite n-silica (right) [61]

According to the surface area and pore size of titanosilicates from several researches, C. Rizzo [62] explained that the surface properties of the various mesoporous titanosilicate were estimated by BET and BJH method. The surface area and pore volume are related to the appearance of cations ( $\text{Na}^+$ ) in pore structure of titanosilicate [62]. Ca, Mg, Sr-EMS-3 has high surface area, and it also has high adsorption capacity. Due to the titanosilicate named EMS-3 was synthesized by using tetramethylammonium hydroxide (TMAOH) in hydrothermal reaction at 7 days and neutralized partial  $\text{OH}^-$  by hydrochloric acid. Moreover, it affect the increased adsorption capacity owing to it has high surface area and pore volume. The surface area and pore volume are given in table 2.6.

Table 2.6 Surface area and pore volume of titanosite [62]

Sample	Specific surface area (m <sup>2</sup> /g)	Pore volume (ml/g)
EMS-3	75	0.341
Ca-EMS-3	440	0.605
Mg-EMS-3	350	0.487
Sr-EMS-3	375	0.434
Ba-EMS-3	210	0.442

A.K. Sinha [63] explained that mesoporous titanosite was used to prepare gold-titanosite catalysts. Therefore, The surface areas of these titanosilicates are between 850 and 1250 m<sup>2</sup>/g [63].

Table 2.7 Surface properties of mesoporous titanosite [63]

Catalyst	Ti/Si	Surface area (m <sup>2</sup> /g)	Pore volume (cm <sup>3</sup> /g)
Ti-MCM-41	0.015	1270.4	1.80
Ti/Ti-MCM-41	0.03	1016.6	0.87
Ti-Meso	0.015	882.9	0.72
TiO-SiO (1)	0.01	891	0.55
TiO-SiO (2)	0.02	834.4	0.86

Furthermore, the large surface area of the titanosite materials affects the increased removal efficiency.

### 2.2.2 Ion exchange mechanism of the sodium titanosite

Sodium titanosite is frequently used for radioactive ions removal due to its resistance with radioactive. Normally, the sodium titanosite is used in adsorption process; however, it also combined with the ion-exchange reaction. Due to the ion-

exchange reaction is the important factor of this material. Na-form of sodium titanate is the predominant factor that leads to enhancement the removal efficiency due to sodium ion as mobile ion, it may be exchanged with metal in solution [64]. Significantly, the sodium titanate is consisted with tetravalent Ti atoms in an octahedral coordination that is generates two negative charges  $(\text{TiO}_6)^{2-}$ , which are balanced by exchangeable sodium ion [65]. Due to the sodium ions in this material has 2 times of titanium and silicon, which is observed from chemical formula.

In this study, the focuses of this study are the Ni adsorption performance using the titanate framework as an adsorbent and its combination with the ion-exchange mechanism of the titanate.

## Chapter 3

### Methodology

In this chapter, the synthesis process and the physical and chemical characterizations before and after Ni adsorption of the sodium titanate are described. The experimental techniques utilized in this thesis to characterize morphology, structure, surface area and functional group will also be outlined.

#### 3.1 Sample preparation

The hydrothermal synthesis methods of the titanate compounds are modified from those reported by Möller *et al* [23]. This is shown in figure 3.1. The abbreviation was given following the synthesis temperature and time. The chemicals used are listed in table 3.1. All chemicals are analytical grade. The abbreviation was given following the synthesis temperature and time. The Teflon-lined vessel was applied with hydrothermal reaction, while plastic beaker was used for reaction at room temperature, are shown in figure 3.2. In this study, the predominant factor was the hydrothermal time and temperature, which are discussed later. Moreover, non-hydrothermal reaction was observed for comparison of the sample characteristic and efficiency.

Table 3.1 List of chemicals that were used in this study

Chemicals	Supplier
Tetraethyl orthosilicate (TEOS, 98%)	ACROS ORGANICS
Titanium (IV) isopropoxide (TIPO, 97%)	SIGMA-ALDRICH
Nickel sulfate ( $\text{NiSO}_4 \cdot 6\text{H}_2\text{O}$ )	AJAX FINECHEM
Sodium hydroxide (NaOH)	MERCK

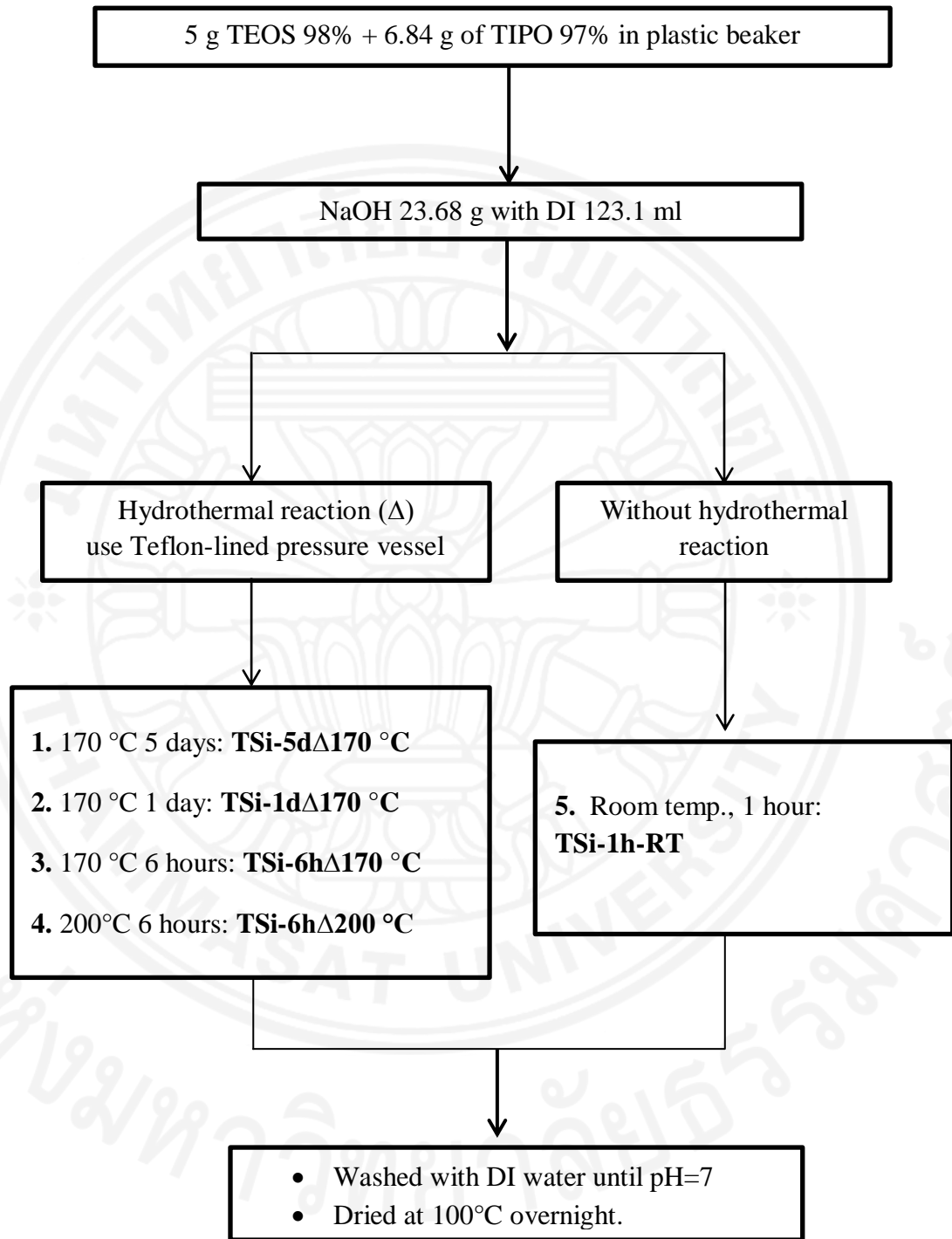


Figure 3.1 Flow chart of the synthesis conditions



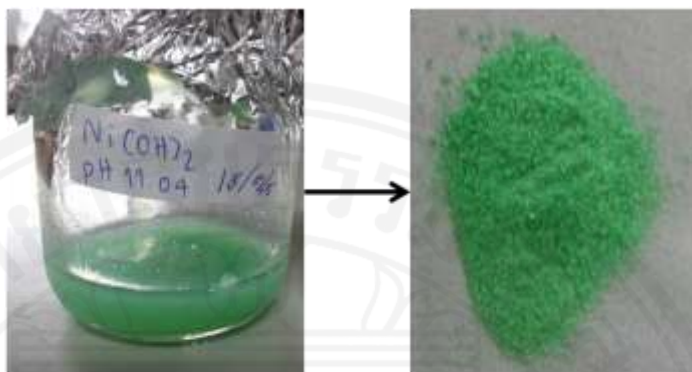


Figure 3. 2 Hydrothermal Teflon-lined pressure vessel (left) and the mixture of precursor reagents in the plastic beaker (right)

### 3.2 The preparation of Ni(OH)<sub>2</sub>

In order to characterize the Ni adsorbed on the adsorbent, reference Ni(OH)<sub>2</sub> powder was also made for comparison using chemical precipitation of Ni(II) solution (1000 mg/l) using NaOH (0.5 M) by adjusting pH of the NiSO<sub>4</sub> solution until pH of 11, the green precipitation is then obtained [66]. The precipitate was washed with demineralized water and then dried at 100°C overnight. The Ni solution used for preparation of Ni(OH)<sub>2</sub> is shown in figure 3.3 A. NiSO<sub>4</sub> powder was obtained from NiSO<sub>4</sub>·6H<sub>2</sub>O and dried at 100°C overnight, small green particles were obtained as shown in figure 3.3 B.

### A) Ni(OH)<sub>2</sub>



### B) NiSO<sub>4</sub>

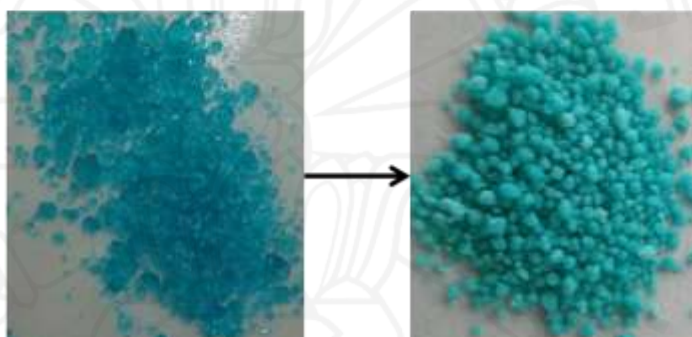


Figure 3.3 Ni (OH)<sub>2</sub> (A) and NiSO<sub>4</sub> powder (B)

## 3.3 Sample characterizations

Samples were characterized using various techniques for investigating the physical and chemical properties of samples.

### 3.3.1 Sample structure

Powder x-ray diffraction (XRD) patterns of samples were obtained using Cu-K $\alpha$  X-radiation with the  $2\theta$  angle from  $10^\circ$  to  $70^\circ$ , and with the step size of  $0.02^\circ$  (PANalytical X'Pert PRO). The accelerating voltage and current used were 40 kV and 30 mA, respectively. XRD equipment was used for the structural analysis of samples before and after Ni adsorption.

### **3.3.2 Samples morphology**

Scanning electron microscopy (SEM) images were obtained using JEOL JSM-5410LV coupled with the Energy Dispersive X-ray Spectrometer (EDS/EDX, Oxford LINK ISIS300) for examination of surface morphology and quantitative elemental information of the adsorbents both before and after adsorption.

### **3.3.3 Sample pore size**

The surface area and pore size of the adsorbents were evaluated using nitrogen gas adsorption on the Autosorb iQ with the BET and BJH analysis models [67]. All samples were outgassed for 20.8 hours at 350°C.

### **3.3.4 Sample functional group**

Fourier-transform infrared (FTIR) spectra of samples were recorded using a Nicolet iS5 ATR spectrometer in the attenuated total reflectance mode. Samples were measured in the range of 3000-525  $\text{cm}^{-1}$ . Molecular structure information and crystal were monitored. The IR spectra of selected adsorbents were compared with the spectra of the  $\text{Ni}(\text{OH})_2$  and  $\text{NiSO}_4$  powder.

### **3.3.5 Heavy metal concentration analysis**

Heavy metal concentrations were analyzed using Inductively Couple Plasma-Optical Emission Spectrometer (ICP-OES), which was obtained on PerkinElmer Optima 8000. The calibration standards were prepared using the stock solution of nickel and stock solution of sodium. The equipment is calibrated using blank solution of deionize water and there are five calibration standards of nickel and sodium such as 1, 10, 250, 500 and 1000  $\text{mg l}^{-1}$  covering interested range of measurement. A linear calibration curve was obtained with the correlation coefficient  $R^2$  greater than 0.999. The samples were automatically measured three times in one aspiration. If the relative standard deviation (RSD) of the results is greater than 1%, the samples were re-measured, or machine re-optimized, until the results have RSD less than 1%.

### 3.4 Batch sorption experiment

The batch adsorption was performed in 30ml plastic bottles at room temperature with agitation speed of 200 rpm.

#### 3.4.1 Sorption capacity

10 mg adsorbents were left in contact with 5 ml of nickel solution at 1, 50, 100, 250, 500, 750 and 1000 mg/l with initial pH value of 5.5 for 24 hours. This experiment was performed in triplicate. After that, the mixture was centrifuged to separate the precipitates from the solution. The precipitates were kept for further characterizations. The Ni solution was analyzed using ICP-OES for evaluation the adsorption performance. In order to obtain the sorption capacity, the amount of ions adsorbed per unit mass of adsorbent,  $q_e$ , in milligrams of metal ions per gram of adsorbent was evaluated using the following expression:

$$q_e = \frac{C_o - C_e}{m} \times V \quad (3.2)$$

where  $C_o$  is the initial metal ion concentration (mg/l),  $C_e$  the equilibrium metal ion concentration (mg/l),  $V$  the volume of the aqueous phase (l), and  $m$  the amount of the adsorbent used (g).

#### 3.4.2 Real wastewater

A real wastewater was obtained from an electroplating industry located in Pathum thani, Thailand. This wastewater was stored in plastic bottle. The initial Ni concentration was 93.4 mg/l, measured by ICP-OES. The pH of the real wastewater was 6.02.

#### 3.4.3 Regeneration and reusability of the selected adsorbents

The used adsorbents were washed with DI water a few times. They were then soaked with 5ml of 0.5M NaOH and shaken at 200 rpm 24 hours. After that, the adsorbents were separated from solution by centrifuged and washed with DI water until the pH of the washed water was about pH 7-8. The regenerated adsorbents were used in Ni removal batch adsorption again. Finally, the concentrations of Ni and Na in the

solution were measured using ICP-OES. The percentage of Ni removal efficiency ( $R$ ) was calculated according to the equation 3.3 [68].

$$R = \frac{C_o - C_e}{C_o} \times 100\% \quad (3.3)$$

## Chapter 4

### Results and discussion

The results of the adsorbent characterizations, which are the morphology, the structure, the functional groups and the surface area, are presented and discussed. Samples that have high Ni removal performance are further selected for regeneration and reusability tests. Characteristics of the adsorbents after regeneration and reuse are also discussed and compared with the freshly synthesized adsorbents. Finally, the performance results of the selected adsorbents in real electroplating wastewater containing both the nickel and chromium ions are also presented and discussed

#### 4.1 Characterization of samples before adsorption

##### 4.1.1 Structural characterization

X-Ray Diffraction (XRD) can be used to provide information regarding crystalline and amorphous structure[69]. The XRD patterns of sodium titanosilicate for different synthesis time of 5 days, 1 day and 6 hours are shown in figure 4.1. Both the 1-day and the 5-day and the 6-hours hydrothermally treated samples have the prominent peak at  $2\theta = 32.75^\circ$  with several smaller peaks that are identified to be at the same positions indicating that they are synthesized into the same crystal structure. Their patterns are well matched with the XRD pattern of natisite ( $\text{Na}_2\text{TiOSiO}_4$ ) (PDF no. 86-1615) [70].

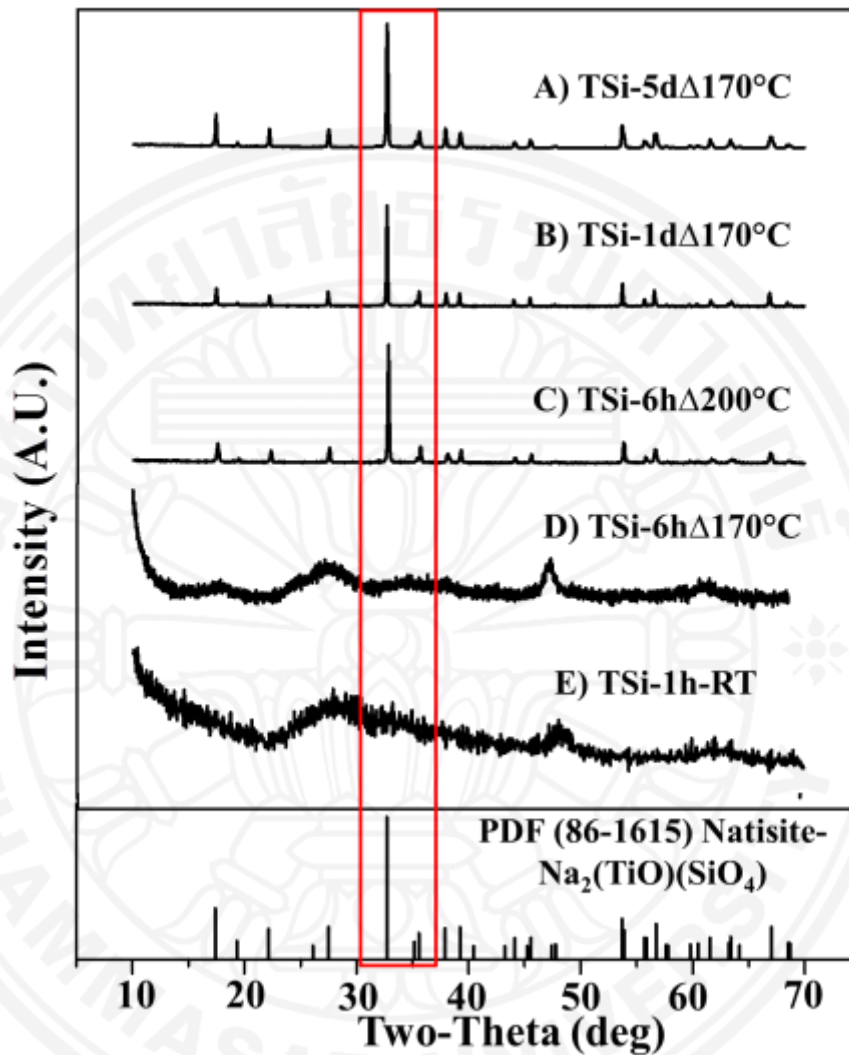


Figure 4.1 XRD pattern of each condition of synthetic adsorbents before Ni adsorption: (A) TSi-5d $\Delta$ 170°C, (B) TSi-1d $\Delta$ 170°C, (C) TSi-6h $\Delta$ 200°C, (D) TSi-6h $\Delta$ 170°C, and (E) TSi-1h-RT

As shown in figure 4.1, the adsorbents may be classified into three categories which are crystalline, semi-crystalline, and amorphous. Crystalline structures are shown in Figure 4.1 (A-C). They show a prominent peak at 32.75°. The intensity of several small peaks is decreased with a decrease in synthesis time. Therefore, this can be indicative that the longest synthesis time of 5 days has the highest crystalline phase formed. Figure 4.1(D) shows semi-crystalline structure where several small peaks of the

titanosilicate phase starts to develop. The XRD pattern of the TSi-1h-RT sample which has not been subjected to hydrothermal treatment shows no prominent peak indicating that this sorbent is still mostly in the amorphous phase. The close up XRD pattern (not shown) of this amorphous sample shows two broad bumps at  $2\theta$  around  $28^\circ$  and  $48^\circ$  indicating combinations of several amorphous titanium and silicon oxides which are known to display small XRD peaks in this region [23].

#### 4.1.2 Morphology characterization

Scanning Electron Microscopy (SEM) is performed to identify the morphological changes of adsorbents in each condition. The morphology results are correlated with structural results, which are presented in figure 4.2. Crystalline structure (figure 4.2 A-C) shows a disc shape. The sample that has the longest hydrothermal time of 5 days consist of several disc shape of size around 5  $\mu\text{m}$  packed or inter grown together into a clam shape ball. For the sample with the 1-day hydrothermal (TSi-1d $\Delta$ 170 $^\circ\text{C}$ ), the adsorbent seems to be consisting of several fine needles and semi-disc shapes that maybe starting to develop into a disc shape similar to that seen in the TSi-5d $\Delta$ 170 $^\circ\text{C}$  (figure 4.2 B).

For sample that has been hydrothermal at higher temperature of 200 $^\circ\text{C}$  (TSi-6h $\Delta$ 200 $^\circ\text{C}$ ) and at shorter time of 6hours, the sample also shows a mixture of the disc-shape, and clamp shell similar to that of (A) and (B).

In addition to the different synthesis time, the hydrothermal temperature is also one factor of the changed morphology. For two samples (figure 4.2 C, D) that have the same the hydrothermal time of 6hours, but these samples have the different synthesis temperature of 170 $^\circ\text{C}$  and 200 $^\circ\text{C}$  (TSi-6h $\Delta$ 170 $^\circ\text{C}$  and TSi-6h $\Delta$ 200 $^\circ\text{C}$ ). The higher temperature of 200 $^\circ\text{C}$  affects the morphology, which shows a mixture of disc-shape and clamp shell. While the morphology of the lower temperature at 170 $^\circ\text{C}$ , does not show any clear or distinct shape to be observed.

For sample without hydrothermal (figure 4.2 E), these sorbents seem to be a large solid with irregular shape or no clear shape.



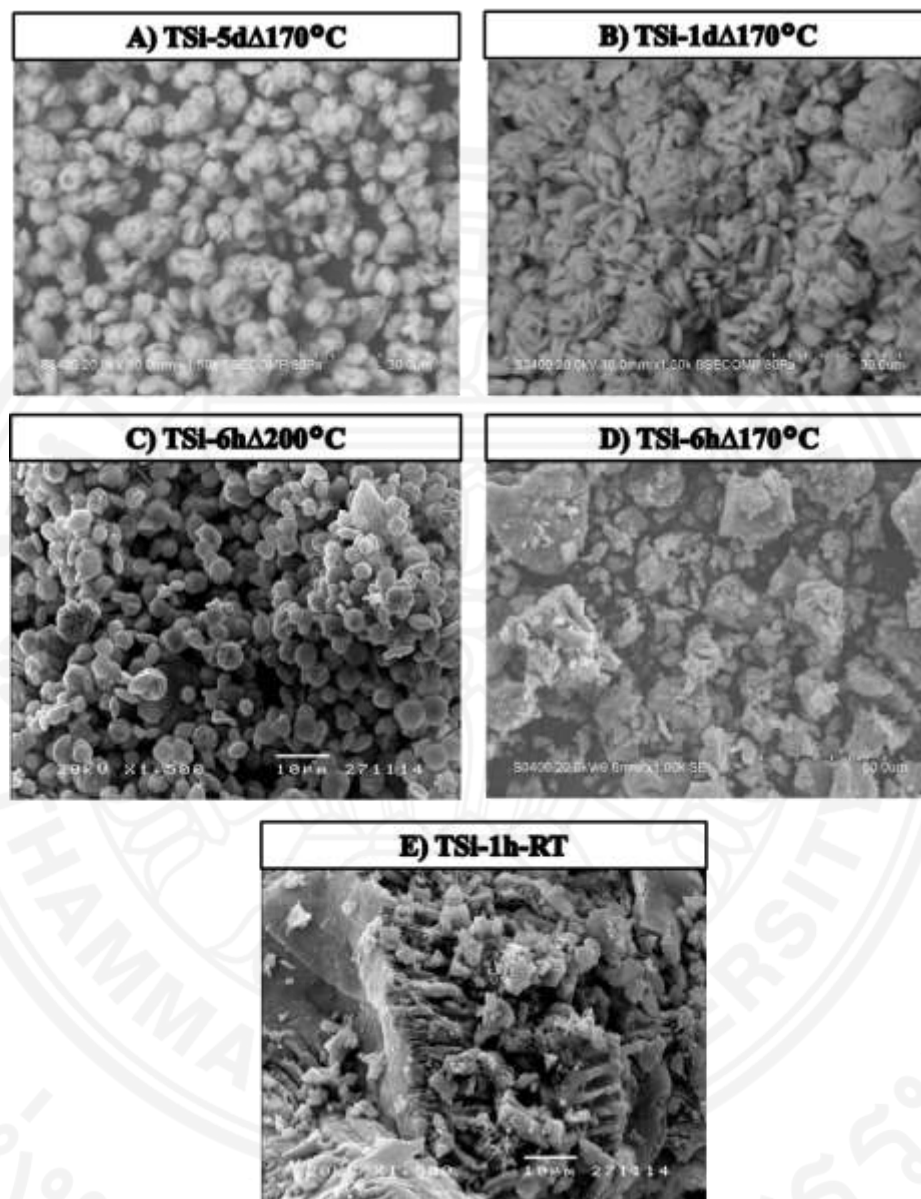


Figure 4.2 SEM images of synthesis adsorbents in each condition before Ni adsorption: (A) TSi-5d $\Delta$ 170 $^{\circ}$ C, (B) TSi-1d $\Delta$ 170 $^{\circ}$ C, (C) TSi-6h $\Delta$ 200 $^{\circ}$ C, (D) TSi-6h $\Delta$ 170 $^{\circ}$ C, and (E) TSi-1h-RT

#### 4.1.3 Functional group characterization

To investigate chemical properties of all samples, Fourier Transform Infrared Spectroscopy in the Attenuated Total Reflectance mode (FTIR-ATR) is used to identify

chemical bonds in the adsorbents. The FT-IR spectra of all samples are presented in figure 4.3. The strong peak at  $880\text{ cm}^{-1}$  may be assigned to the Ti-O-Si vibration [71], and two relative sharp bands at  $725$  and  $624\text{ cm}^{-1}$  may be assigned to the internal vibration modes of  $\text{TiO}_5$  (normal) and  $\text{SiO}_4$  structural units, respectively [60]. When the hydrothermal time is decreased from 5 days to 1 day and 6 hours (figures 4.3 A-D), the characteristic peaks of natisite at  $624$  and  $725\text{ cm}^{-1}$  appear to be lower and broader than those of the TSi-5d $\Delta$ 170°C indicating that the  $\text{TiO}_5$  and the  $\text{SiO}_4$  structural units may not have fully crystallized into rigid framework. This FTIR result is also in the same trend as that in the XRD results.

The sample that has been hydrothermally treated at higher temperature of  $200^\circ\text{C}$  but at shorter time (TSi-6h $\Delta$ 200°C) also shows similar peaks to the TSi-5d $\Delta$ 170°C and TSi-1d $\Delta$ 170°C but slightly lower intensity.

Furthermore, the samples that are predominantly amorphous (TSi-6h $\Delta$ 170°C and TSi-1h-RT) show only the small peak at  $890\text{ cm}^{-1}$  and the slight hump at  $624\text{ cm}^{-1}$ . This is indicative of the natisite phase that is starting to develop due to the weak presence of Ti-O-Si bonds.

These XRD, SEM and FTIR results point in the same trend that the longer the hydrothermal time, or the higher hydrothermal temperature lead to higher crystalline content of the adsorbent samples.

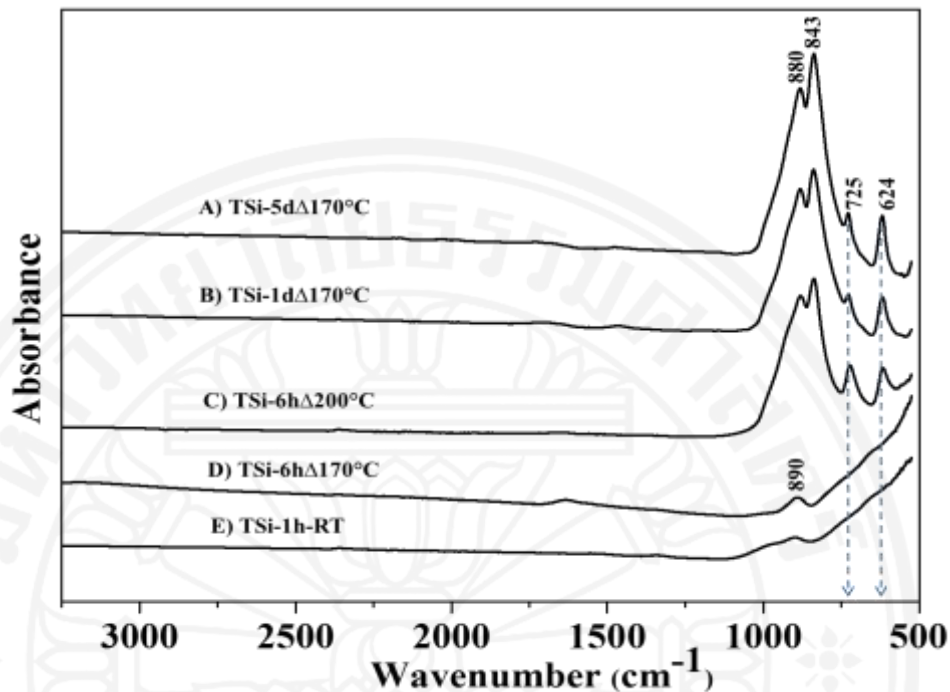


Figure 4.3 FTIR spectra of synthesis adsorbents: (A) TSi-5dΔ170°C, (B) TSi-1dΔ170°C, (C) TSi-6hΔ200°C, (D) TSi-6hΔ170°C, and (E) TSi-1h-RT

## 4.2 Adsorption isotherm

### 4.2.1 Sorption Capacity

The analysis of sorption capacity data is important to develop an equation which accurately represents the results and which could be used for design purposes and used for select the adsorbent to be representative of each structure. To investigate the Ni sorption capacity of each adsorbent, the adsorption isotherm which is plot between the equilibrium Ni concentrations in the solution ( $C_e$ ) and the equilibrium amount of Ni adsorbed onto the sorbent ( $Q_e$ ) at various Ni concentrations was plotted as shown in figure 4.4.

Langmuir model is one of the isotherms that can be used to estimate the maximum adsorption capacity of the adsorbent. This model is about the adsorption onto the homogeneous surfaces materials [72]. It is based on describing the sorption as a monolayer adsorption [73]. The Langmuir model can be expressed as:

$$Q_e = \frac{Q_{max} K_L C_e}{1 + K_L C_e} \quad (4.1)$$

where  $Q_{max}$  is the maximum adsorption capacity of the sorbent (mg/g) and  $K_L$  is the affinity constant for Ni of the adsorbent (l/mg). The experimental data,  $Q_{max}$ ,  $K_L$ , and  $R^2$ , of each adsorbent are given in table 4.2.

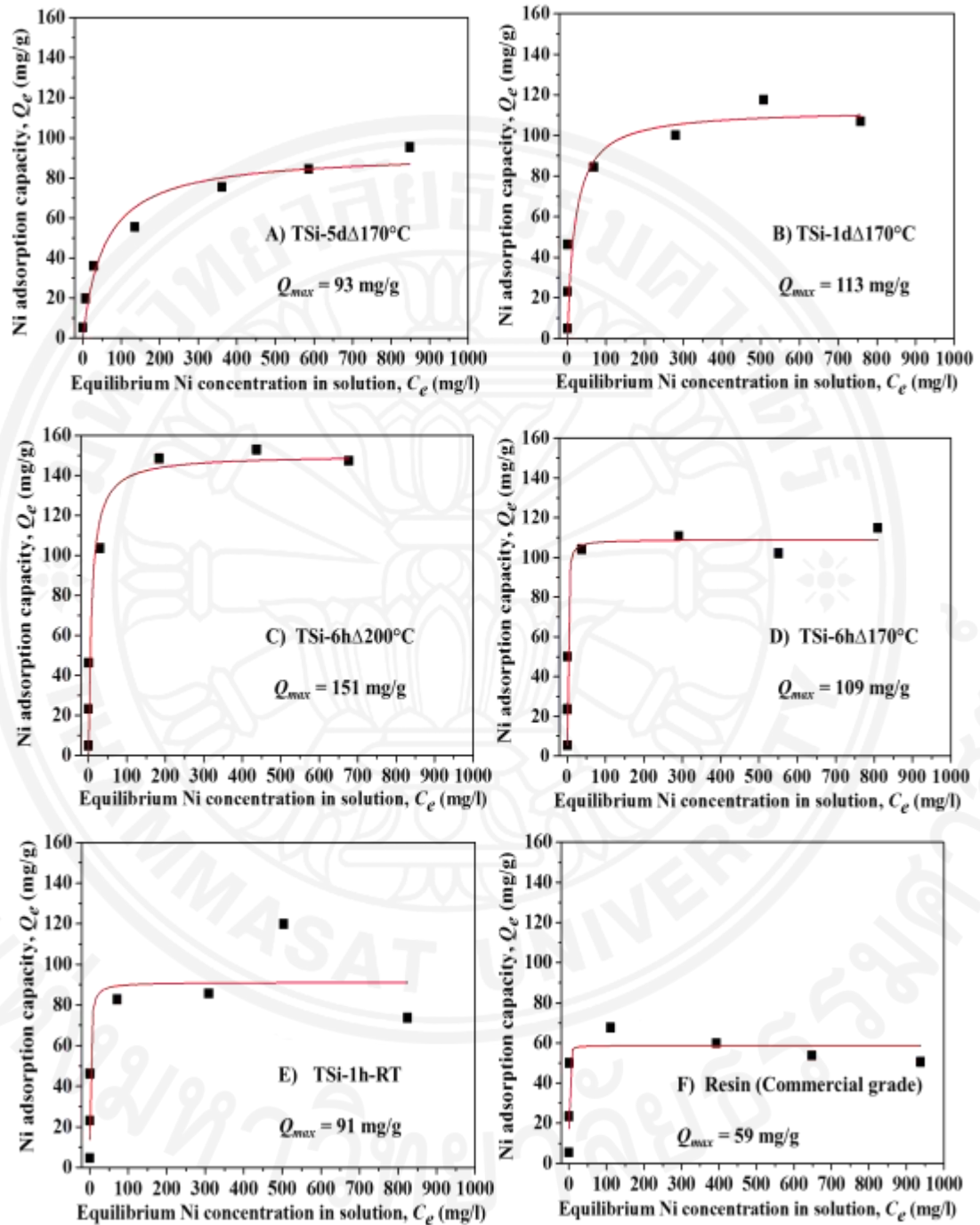


Figure 4.4 Fitting of Langmuir model (Eq.4.1) to plot evaluate maximum Ni adsorption capacity: (A) TSi-5d $\Delta$ 170°C, (B) TSi-1d $\Delta$ 170°C, (C) TSi-6h $\Delta$ 200°C, (D) TSi-6h $\Delta$ 170°C, (E) TSi-1h-RT, and (F) Resin

Figure 4.4 shows the TSi-5d $\Delta$ 170 $^{\circ}$ C (figure 4.4A) seems to be able to fit the Langmuir model quite well. From the structure of the adsorbents, the crystalline structures seem to be able to be fitted with the Langmuir model better than those of the amorphous structure.

For the Langmuir parameters, table 4.1 shows the maximum adsorption capacity ( $Q_{max}$ ) of the adsorbents, which can be compared with commercial grade resin. This result is the preliminary result of the Ni adsorption in order to select the representative adsorbents that have high the adsorption capacity. Moreover, this result shows the Ni adsorption performance of the sodium titanosilicate is also higher than that of the commercial grade resin (Plurolite  $\text{\textcircled{R}}$ ). The maximum adsorption capacity ( $Q_{max}$ ) of resin is the lowest at 59 mg Ni/g resin and  $Q_{max}$  of TSi-6h $\Delta$ 200 $^{\circ}$ C is the highest at 151 mg Ni/g sorbent. The selected adsorbent adsorption isotherms are plotted together again for comparison and is shown in figure 4.5.

Table 4.1 Langmuir isotherms of synthesis adsorbents is compared with resin (commercial grade)

Adsorbents	Structure	Langmuir isotherm		
		$Q_{max}$ (mg/g)	$K_L$ (l/mg)	$R^2$
1.TSi-5d $\Delta$ 170 $^{\circ}$ C	Crystalline	93	0.002	0.946
2.TSi-1d $\Delta$ 170 $^{\circ}$ C		113	0.050	0.629
3.TSi-6h $\Delta$ 200 $^{\circ}$ C		151	0.121	0.891
4.TSi-6h $\Delta$ 170 $^{\circ}$ C	Amorphous	109	0.995	0.879
5.TSi-1h-RT		91	0.655	0.732
6.Commercial resin		59	3.356	0.692

According to Ni adsorption of all adsorbents, the selected adsorbents which have the highest Ni adsorption capacities are chosen to be representative of the sodium

titanosilicate in this study. The adsorption isotherms of these selected adsorbents are repeated again (triplicate) to ensure representative adsorption isotherms are obtained.

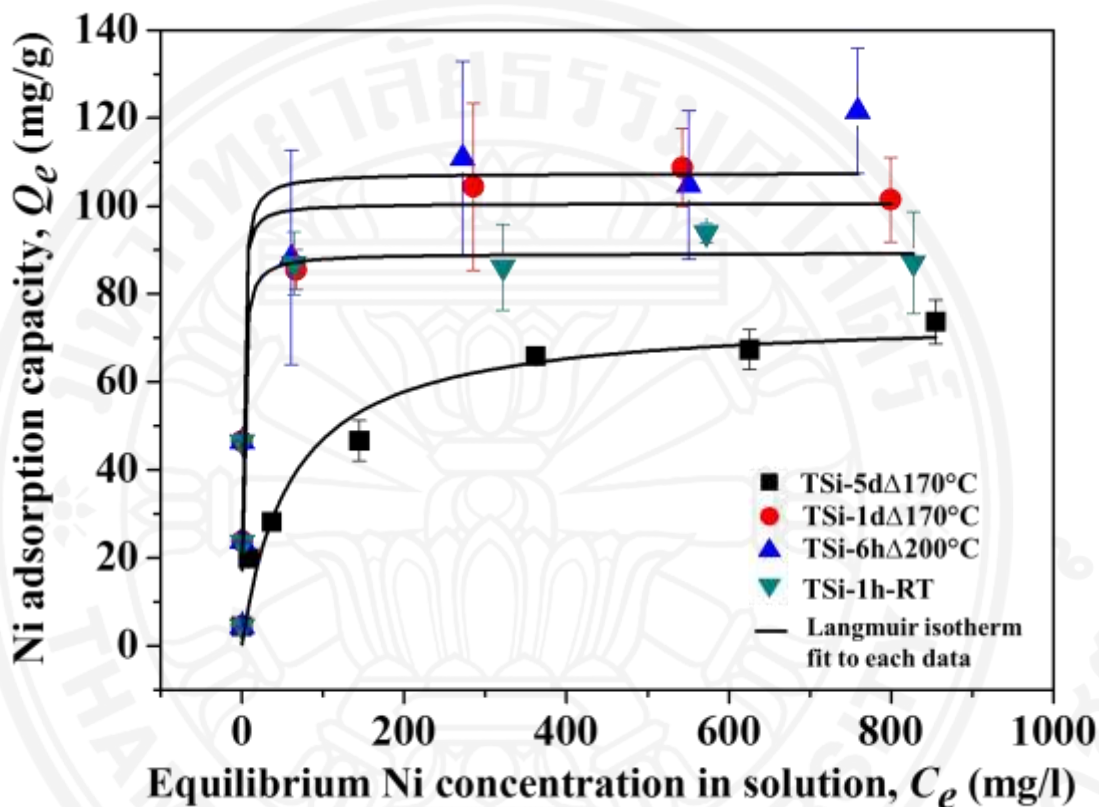


Figure 4.5 Experimental data of the selected adsorbents fitted with the Langmuir model.

The parameters of the Langmuir model are shown in table 4.2. TSi-6h $\Delta$ 200 $^{\circ}$ C has the highest nickel adsorption capacity at 108 mg Ni/g sorbent. The TSi-5d $\Delta$ 170 $^{\circ}$ C that has the highest crystallinity that has the lowest nickel adsorption capacity at 75 mg Ni/g sorbent due to their pore volume is quite low when compared with other samples (see discussion on surface area and pore volume in section 4.4). The hydrate ions probably cannot diffuse into the channels inside the adsorbents [28]. The sample TSi-1h-RT without hydrothermal treatment also shows the Ni adsorption capacity of about 85 mg Ni/g. There seems to be an optimal condition in terms of the hydrothermal treatment that can result in high Ni sorption of the synthesized sorbents.

In addition, the Langmuir constant ( $K_L$ ) of the selected adsorbents is shown in table 4.2. The value of  $K_L$  of TSi-5d $\Delta$ 170°C is 0.016 l/mg followed by TSi-1h-RT, TSi-6h $\Delta$ 200°C, and TSi-1d $\Delta$ 170°C is 0.634, 0.687, and 1.029 l/mg, respectively. The Langmuir constant is related to the energy of adsorption in all sites [74, 75]. The high value of the Langmuir constant can be indicative of the strength of adsorption [76] and the high affinity of the sorbent for the sorbate [75]. In this case, the TSi-1d $\Delta$ 170°C has the highest affinity for the nickel although its capacity is slightly lower than that of the TSi-6h $\Delta$ 200°C. For treating low concentration of Ni, TSi-1d $\Delta$ 170°C will adsorb Ni better than other adsorbents due to its strong affinity for Ni.

The sample with the highest crystallinity (TSi-5d $\Delta$ 170°C) may have too rigid the pore structure that does not allow easy sorption of Ni into the structure, while the amorphous sample (TSi-1h-RT) without the hydrothermal treatment may have too large the grain size (as seen in the SEM image above) that does not allow efficient diffusion or exchange of Ni ions into the sorbent structure. The ion exchange of Ni<sup>2+</sup> with Na<sup>+</sup> ions is shown in the next section.

Table 4.2 Langmuir parameters of the selected adsorbents

Adsorbents	$Q_{max}$ (mg/g)	$K_L$ (l/mg)	$R^2$
1. TSi-5d $\Delta$ 170°C	75	0.016	0.947
2. TSi-1d $\Delta$ 170°C	101	1.029	0.885
3. TSi-6h $\Delta$ 200°C	108	0.687	0.889
4. TSi-1h-RT	89	0.634	0.899

### 4.3 Ion exchange mechanism between Ni<sup>2+</sup> in solution Na<sup>+</sup> on adsorbents

The synthesized sodium titanosilicate compounds are expected to remove Ni through the ion-exchange mechanism with sodium in the zeolite-like sodium titanosilicate structure. The exchangeability of Na<sup>+</sup> and Ni<sup>2+</sup> is investigated by calculating the mole ratio of Ni<sup>2+</sup>/Na<sup>+</sup>. Na<sup>+</sup> ions are released from the structure of the adsorbent into



the Ni solution, whereas the Ni<sup>2+</sup> ions are adsorbed onto the adsorbent, in a mole ratio that is close to two. The Na<sup>+</sup> ion is monovalent, and a Ni<sup>2+</sup> ion is divalent.

Table 4.3 shows the calculated mole ratio of the initial nickel concentration, 50-1000 mg/l. The mole ratio between the Na<sup>+</sup> and Ni<sup>2+</sup> is calculated and displayed in the last column. They are very close to the ideal ratio of 2 for all sorbents indicating that the predominant Ni removal mechanism in all these sorbents are mainly through the ion-exchange mechanism. Moreover, at low concentrations of Ni, the ratios observed in all sorbents were higher than two because of not enough of the Ni in the surrounding solutions, and that the sodium in the sorbents exchanged with the hydronium ions of the surrounding water, resulting in the mole ratio of the released Na ions to the adsorbed Ni larger than two.

Table 4. 3 Mole ratio of Na<sup>+</sup> in solution and Ni<sup>2+</sup> onto each selected adsorbent: (A) TSi-5dΔ170°C, (B) TSi-1dΔ170°C, (C) TSi-6hΔ200°C, and (D) TSi-1h-RT (M.W. of Ni = 58.69 g/mole, M.W. of Na = 22.99 g/mole)

A) TSi-5dΔ170°C

Conc. (mg/l)	C <sub>e</sub> (mg/l)		Weight (g)		Mole		Mole ratio Na <sup>+</sup> /Ni <sup>2+</sup>
	Ni	Na	Ni	Na	Ni	Na	
50	8.34	41.39	1.98E-04	2.07E-04	3.38E-06	9.00E-06	2.66
100	36.99	55.30	2.82E-04	2.77E-04	4.80E-06	1.20E-05	2.51
250	144.63	76.57	4.66E-04	3.83E-04	7.93E-06	1.67E-05	2.10
500	362.30	99.84	6.59E-04	4.99E-04	1.12E-05	2.17E-05	1.94
750	625.50	102.43	6.74E-04	5.12E-04	1.15E-05	2.23E-05	1.94
1000	854.70	118.10	7.37E-04	5.91E-04	1.25E-05	2.57E-05	2.05

**B) TSi-1dΔ170°C**

Conc. (mg/l)	$C_e$ (mg/l)		Weight (g)		Mole		Mole ratio $\text{Na}^+/\text{Ni}^{2+}$
	Ni	Na	Ni	Na	Ni	Na	
50	0.47	49.17	2.38E-04	2.46E-04	4.05E-06	1.07E-05	2.64
100	0.30	79.26	4.65E-04	3.96E-04	7.92E-06	1.72E-05	2.18
250	66.75	139.33	8.55E-04	6.97E-04	1.46E-05	3.03E-05	2.08
500	285.20	160.43	1.04E-03	8.02E-04	1.78E-05	3.49E-05	1.96
750	542.63	157.60	1.09E-03	7.88E-04	1.85E-05	3.43E-05	1.85
1000	799.13	155.70	1.01E-03	7.79E-04	1.73E-05	3.39E-05	1.96

**C) TSi-6hΔ200°C**

Conc. (mg/l)	$C_e$ (mg/l)		Weight (g)		Mole		Mole ratio $\text{Na}^+/\text{Ni}^{2+}$
	Ni	Na	Ni	Na	Ni	Na	
<b>50</b>	0.49	55.36	2.38E-04	2.77E-04	4.05E-06	1.20E-05	2.97
<b>100</b>	0.48	89.06	4.64E-04	4.45E-04	7.91E-06	1.94E-05	2.45
<b>250</b>	61.19	156.20	8.83E-04	7.81E-04	1.50E-05	3.40E-05	2.26
<b>500</b>	272.17	180.13	1.11E-03	9.01E-04	1.89E-05	3.92E-05	2.07
<b>750</b>	550.60	167.60	1.05E-03	8.38E-04	1.79E-05	3.65E-05	2.04
<b>1000</b>	758.77	210.00	1.22E-03	1.05E-03	2.07E-05	4.57E-05	2.20

**D) TSi-1h-RT**

Conc. (mg/l)	$C_e$ (mg/l)		Weight (g)		Mole		Mole ratio $\text{Na}^+/\text{Ni}^{2+}$
	Ni	Na	Ni	Na	Ni	Na	
50	0.91	51.30	2.36E-04	2.57E-04	4.01E-06	1.12E-05	2.78
100	0.68	94.17	4.63E-04	4.71E-04	7.89E-06	2.05E-05	2.59
250	63.96	150.83	8.69E-04	7.54E-04	1.48E-05	3.28E-05	2.22
500	321.77	141.90	8.61E-04	7.10E-04	1.47E-05	3.09E-05	2.10
750	572.43	144.17	9.39E-04	7.21E-04	1.60E-05	3.14E-05	1.96
1000	827.70	157.40	8.72E-04	7.87E-04	1.48E-05	3.42E-05	2.31

#### 4.4. Surface area and pore size of the selected adsorbents

In this section, the surface areas of the selected adsorbents before Ni adsorption are analyzed using BET in order to explain the reasons of the maximum adsorption capacity of the selected adsorbents.

Brunauer-Emmett-Teller (BET) is a technique that is used to analyze surface area by nitrogen multilayer adsorption. The results are given in table 4.4. Microporous structure will have pore diameter less than 2nm [77]. Macroporous structure has pore diameter larger than 50 nm, and the pore diameter of the mesoporous structure is between 2 nm and 50 nm [78]. As a result, all of the selected adsorbents in this study can be classified as having mesoporous structure due to their pore diameter in range from 3 nm to 12 nm. The surface area of the crystalline adsorbents is related to the maximum adsorption capacity and the appearance of Na<sup>+</sup> ions in the structure [62], which is observed by EDS result in table 4.5. The semi-crystalline structure, TSi-6hΔ200°C, has the highest pore volume and surface area at 0.108 cm<sup>3</sup>/g and 63.536 m<sup>2</sup>/g, respectively. It also has the highest adsorption capacity of 108 mg Ni/g sorbent. Meanwhile the amorphous adsorbent, TSi-1h-RT, has the lowest pore volume at about 0.027 cm<sup>3</sup>/g owing possibly to the bonding of the Na<sup>+</sup> ions and water molecules in their cavities which occurs in disordered arrangement [59].

Table 4.4 BET results of selected adsorbents from BJH model

<b>Selected adsorbents</b>	<b>Pore diameter (nm)</b>	<b>Pore volume (cm<sup>3</sup>/g)</b>	<b>Surface area (m<sup>2</sup>/g)</b>	<b><i>Q</i><sub>max</sub> (mg/g)</b>
TSi-5dΔ170°C	4.903	0.055	39.924	75
TSi-1dΔ170°C	3.409	0.054	43.205	101
TSi-6hΔ200°C	3.827	0.108	63.536	108
TSi-1h-RT	12.287	0.027	6.632	89

## 4.5 Characterization of selected adsorbent after Ni adsorption

### 4.5.1 Structural characterization

Figure 4.6 shows the comparison of XRD patterns of the selected adsorbent after adsorption with those before adsorption. In all samples after adsorption, no new phases due to Ni adsorption can be identified in these patterns, only the decrease in the peak intensity can be observed. These patterns are measured using the same conditions, and plotted without any scaling. Based on the XRD intensity, it can be seen that after adsorption, the crystalline phase of the TSi-6h $\Delta$ 200 $^{\circ}$ C is lost compared to that of the TSi-1d $\Delta$ 170 $^{\circ}$ C sample where the crystallinity is still retained. The XRD intensity shown can be used roughly to indicate the relative amount of the crystalline phase in the adsorbents that contribute to the XRD patterns. The structure of the TSi-6h $\Delta$ 200 $^{\circ}$ C (figure 4.2C) has the most change, owing possibly to the high loading of Ni ion into the structure and also the release of Na ion from the structure leading to loss of crystallinity and possibly collapse of structure.

For the amorphous sample, TSi-1h-RT (figure 4.2 D), XRD pattern shows no significant changes after adsorption, and no new phase of nickel compounds could be detected.

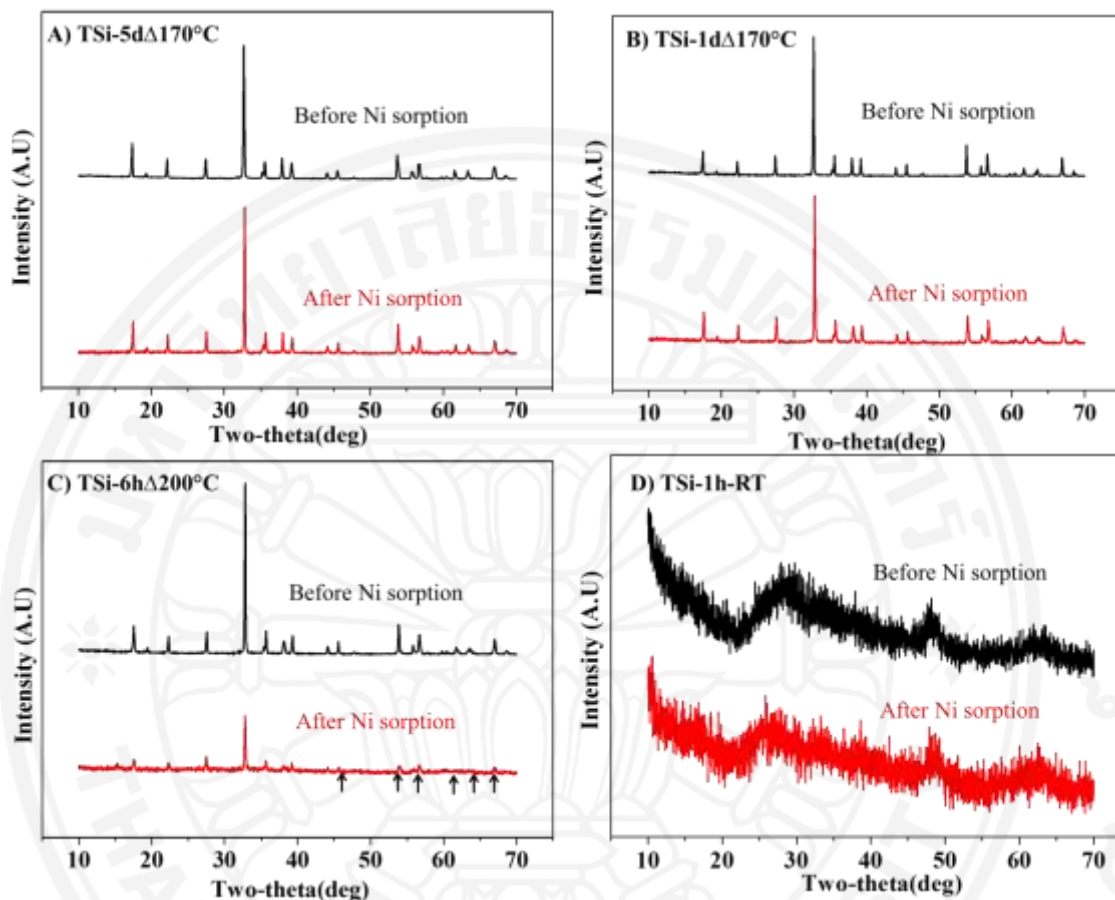


Figure 4.6 XRD patterns of the selected adsorbents before and after adsorption: (A) TSi-5d $\Delta$ 170 $^{\circ}$ C, (B) TSi-1d $\Delta$ 170 $^{\circ}$ C, (C) TSi-6h $\Delta$ 200 $^{\circ}$ C, and (D) TSi-1h-RT

#### 4.5.2 Morphology characterization

The morphology of the selected adsorbents after Ni adsorption in comparison with those before adsorption is shown in figure 4.7. The morphology results are related to the structural results. The corrosion of the adsorbents can also be observed in the XRD patterns of the adsorbents.

Figure 4.7 shows the morphology of the selected adsorbents after Ni adsorption. The morphology of Af-TSi-5d $\Delta$ 170 $^{\circ}$ C, which is the highest crystalline content, is observed to be similar to the shape of the freshly synthesized samples except that the adsorbents may be somewhat rounder and more packed together.

For the sample with 1 day, Af-TSi-1d $\Delta$ 170°C seems to have been corroded with some small pieces showing up on the surface. For the sample TSi-6h $\Delta$ 200°C, the disc-shape adsorbent after Ni adsorption is clearly seen to be corroded into a mixture of small amount of disc shape and some irregular shape.

For the amorphous sample, Af-TSi-1h-RT still looked like irregular chunk of solids similar to that before adsorption.

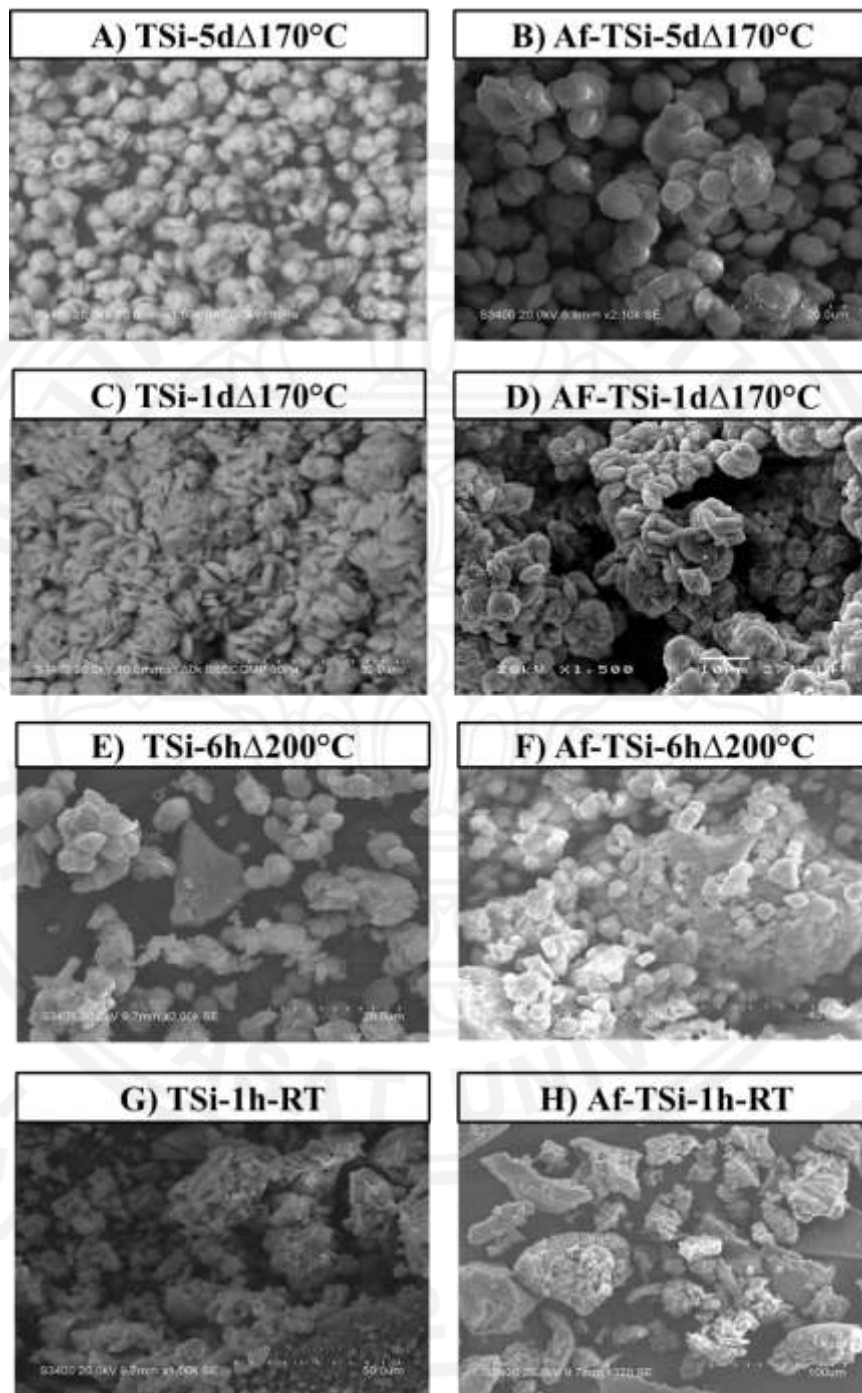


Figure 4.7 SEM images of the selected adsorbents before (left) and after (right) adsorption. From top to bottom: TSi-5d $\Delta$ 170 $^{\circ}$ C, TSi-1d $\Delta$ 170 $^{\circ}$ C, TSi-6h $\Delta$ 200 $^{\circ}$ C, and TSi-1h-RT

### 4.5.3 Elemental composition characterization

The chemical properties of the selected adsorbents are characterized by using Energy-dispersive X-ray spectroscopy (EDS) for analyzing elements on surface of the selected adsorbents. As seen in table 4.5, the major elements are chosen to compare between before (Bf) and after (Af) Ni adsorption. Moreover, the other elements are V and Ba (not shown in this Table) that is shown in very low amount, which means the insignificant elements.

Table 4.5 Elements (% weight) on surface of the selected adsorbent (Bf : Before Ni adsorption, and Af : After Ni adsorption)

Selected adsorbents	Elements (% weights)					
	C	O	Na	Si	Ti	Ni
	Bf/Af	Bf/Af	Bf/Af	Bf/Af	Bf/Af	Af
TSi-5d $\Delta$ 170°C	11.2/18.0	51.9/50.7	9.0/3.4	7.5/5.0	20.4/13.4	9.4
TSi-1d $\Delta$ 170°C	11.8/15.9	53.4/49.3	8.7/4.7	7.2/4.0	18.9/13.9	12.9
TSi-6h $\Delta$ 200°C	-	39.9/35.5	17.3/7.4	11.2/7.6	31.2/22.0	23.2
TSi-1h-RT	12.2/0	53.6/36.4	4.7/1.3	1.2/1.8	26.2/37.3	18.3

The table above illustrates elements on surface of the selected adsorbents, which are compared between before and after Ni adsorption. This result shows that the most amount of Ni on surface of TSi-6h $\Delta$ 200°C is 23.2 % weight. Beside this adsorbent, TSi-5d $\Delta$ 170°C has the Ni on surface at 9.4% weight followed by TSi-1d $\Delta$ 170°C, and TSi-1h-RT is 12.9, and 18.3 % weight, respectively. The amounts of Ni on surface are related to the maximum adsorption capacity ( $Q_{max}$ ), which is shown in table 4.2. The highest adsorption capacity also has the highest % of Ni on surface.



Besides the amount of Ni when after Ni adsorption, the percentage of Si of TSi-1h-RT is the lowest element whereas the percentages of Ti is the highest element because the slow reaction at 1 hour does not enough to form the titanosilicate as adsorbent completely. This result may be related to the functional group result, which is composed of the sodium titanosilicate.

#### 4.5.4 Functional group characterization

FTIR spectra of the selected adsorbents after Ni adsorption in comparison with those before adsorption are given in figure 4.8. This result also shows the collapse of the crystal structure, that may be occurred by the charge and size mismatched of the  $\text{Ni}^{2+}$  ion. It may cause large electric field inside the structure, leading to instability of the structure[79].

The prominent peak of sodium titanosilicate at  $888\text{ cm}^{-1}$  which is assigned to the vibration of Ti-O-Si [71] and the relative sharp peak at  $725\text{ cm}^{-1}$  and  $624\text{ cm}^{-1}$  may be assigned to the vibration modes of  $\text{TiO}_5$  and  $\text{SiO}_4$ , respectively [60], and this also can be an indicative of the crystalline characteristic.

For the sample, TSi-5d $\Delta$ 170°C (figure 4.8 A), still retains some crystalline after adsorption while the other crystalline samples, TSi-1d $\Delta$ 170°C and TSi-6h $\Delta$ 200°C (figure 4.8 B-C), show very little of the two peaks left implying that the  $\text{TiO}_5$  and  $\text{SiO}_4$  may have been destroyed.

The new peak at  $1118\text{ cm}^{-1}$ , which is shown in all adsorbent after Ni adsorption, is assigned to the sulfate peak that came from the residual of  $\text{NiSO}_4$  used in the Ni stock solution [80]. The peaks around  $1654\text{ cm}^{-1}$  are assigned to the -OH vibration from the adsorbed water molecules. The weak peak at  $1252\text{ cm}^{-1}$  is assigned to sulfur trioxide ( $\text{SO}_3$ ) [81]. Both  $\text{SO}_3$  and  $\text{SO}_4$  are probably caused from the component in nickel sulfate ( $\text{NiSO}_4$ ) solution. For the sample, TSi-1d $\Delta$ 170°C (figure 4.8 B), shows the peak at  $805\text{ cm}^{-1}$  that is assigned to the symmetric stretching Si-O-Si [82], and the peak at  $667\text{ cm}^{-1}$  is observed to the vibration of Ti-O-Ti bonds [83].

The loss of the crystallinity after Ni exchange, that is likely due to the collapse of the crystalline structure of natisite upon the exchange of the  $\text{Na}^+$  with the  $\text{Ni}^{2+}$  ions.

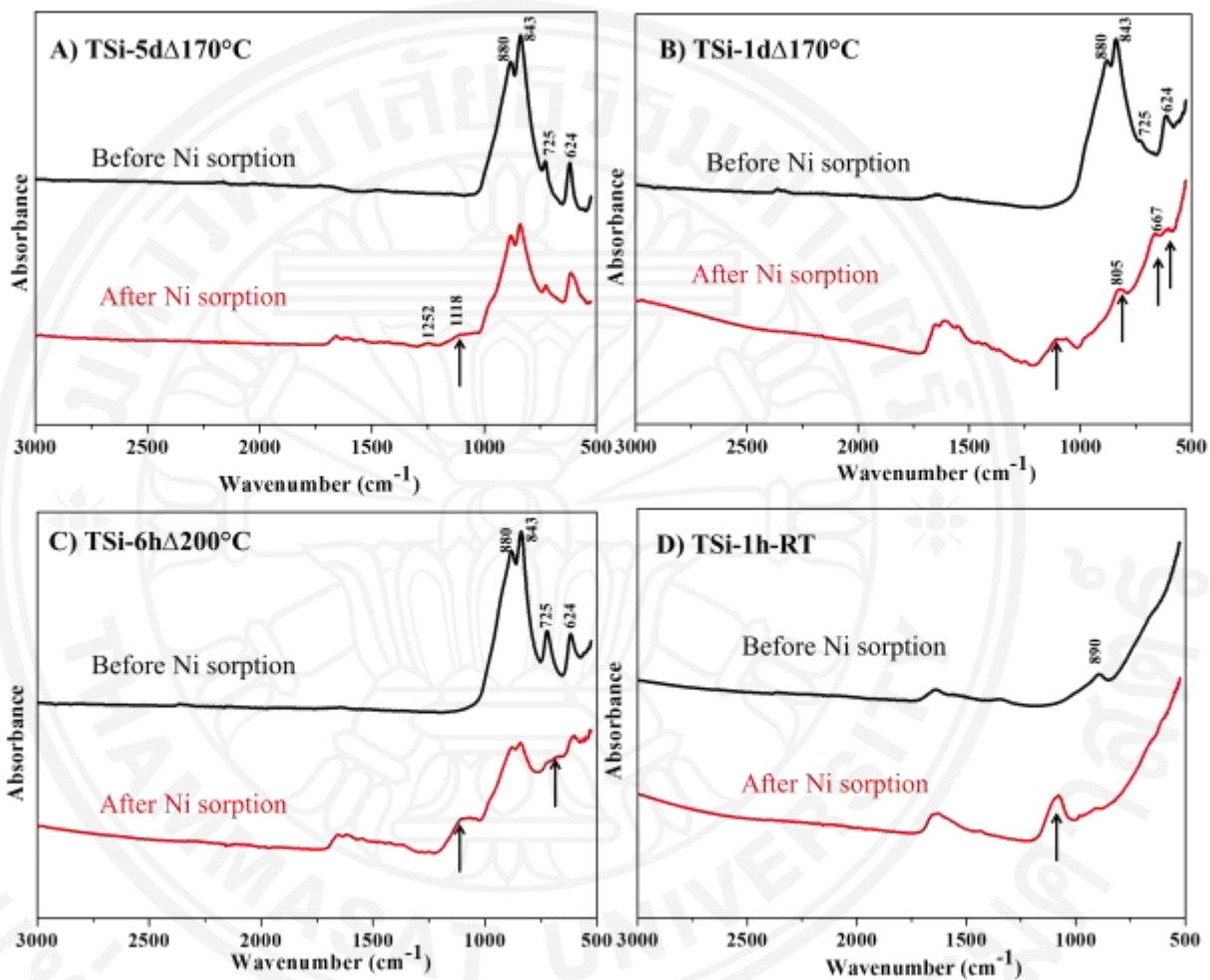


Figure 4.8 FTIR spectra of the selected adsorbents before and after Ni adsorption: (A) TSi-5d $\Delta$ 170 $^{\circ}$ C, (B) TSi-1d $\Delta$ 170 $^{\circ}$ C, (C) TSi-6h $\Delta$ 200 $^{\circ}$ C, and (D) TSi-1h-RT. The arrows are at 888, 843, 725, and 624  $\text{cm}^{-1}$  correspond to peak positions in the pristine crystalline samples shown earlier, while those at 1252 and 1118  $\text{cm}^{-1}$  corresponded to that of the sulfate group of the  $\text{NiSO}_4$  solution used.

For comparison, Figure 4.9 only shows FTIR spectra of the selected adsorbents after Ni adsorption in comparison with the FTIR spectra of the  $\text{NiSO}_4$  powder [80], that is used in preparation of the Ni stock solution. This result can be confirmative the sulfate peak at  $1118\text{ cm}^{-1}$  that came from the use of  $\text{NiSO}_4$  in the stock solution.

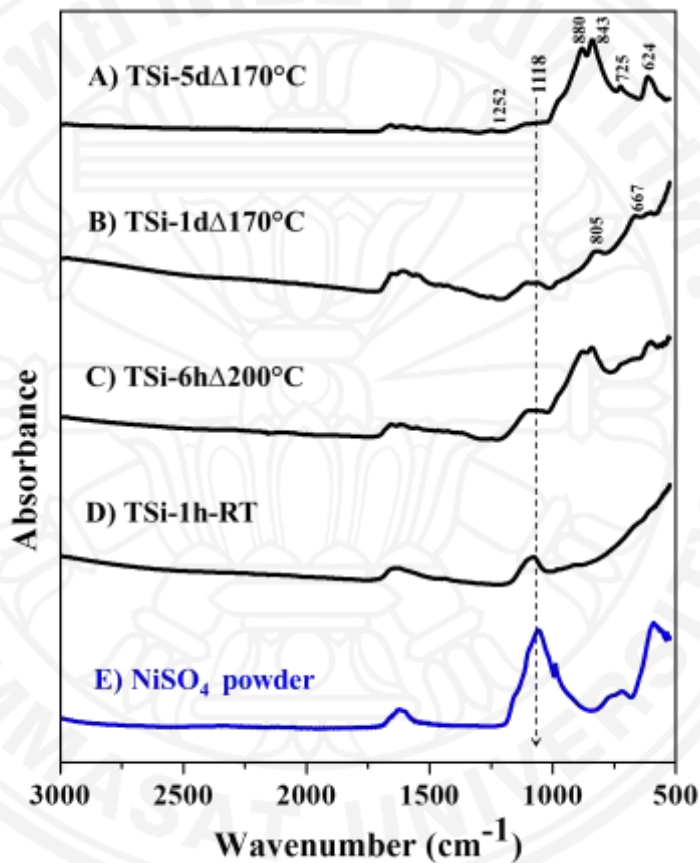


Figure 4.9 FTIR spectra of selected adsorbents after Ni adsorption are compared with the spectra of the  $\text{NiSO}_4$  powder.

#### 4.6 Regeneration and reusability of the selected adsorbents

In this section, the selected sorbents are also tested for their ability to be regenerated. The sodium hydroxide ( $\text{NaOH}$ ) of 0.5 M is used for regeneration the adsorbents by continuous shaking. After that, the adsorbents are reused for Ni adsorption at initial Ni concentrations of  $1000\text{ mg/l}$  in all subsequent reuse cycles. The Ni removal efficiency of each adsorbent after each cycle of used is reported.

#### 4.6.1 Removal efficiency of selected adsorbent after regeneration

Figure 4.10 shows the Ni removal efficiency of the selected adsorbents which is calculated using equation 3.3 in each cycle. The selected adsorbents are recovered with the improvement in the Ni removal efficiency. The improvement of the increased regeneration efficiency is rather surprising. Because it is possible that some NaOH may still be left in the adsorbent structure and react with the Ni ions resulting in the  $\text{Ni(OH)}_2$  precipitation and a higher Ni removal efficiency. The solution color after regeneration has become transparent green indicating that Ni has been successfully removed from the adsorbent into the NaOH solution imparting the usual green color.

Beside the remains of NaOH, the crystalline structures have increased removal efficiency in the second and the third time; however, the amorphous has the significantly decreased removal efficiency in a second time. The amorphous structure may be damaged after Ni adsorption; however, this can be reacted with NaOH during the regeneration and its resulting in some phases of titanate may be occurred when treated with NaOH, that is the reason why the removal efficiency of amorphous adsorbent in a third time is increased up to nearly the first time of adsorption.

The characteristics of the selected adsorbents are one factor that is resulting in the improvement of the removal efficiency, which is discussed later.

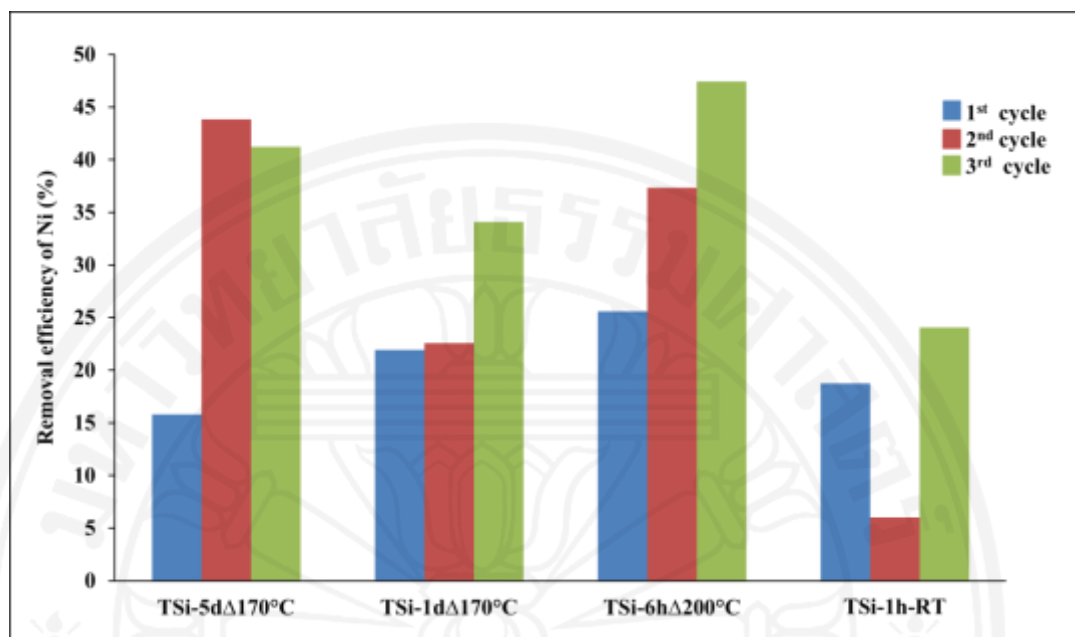


Figure 4. 10 Removal efficiency of Ni of select adsorbents in three cycles

#### 4.6.2 Characteristics of selected adsorbents after regeneration and reusability

The morphologies and functional group of the selected adsorbents after regeneration and second reuse are readily characterized using SEM and FTIR-ATR, respectively. This can be indicative of the effect of the increasing removal efficiency.

##### 4.6.2.1 The morphology of the selected adsorbents

After the selected adsorbents is regenerated and reused in second time, these processes affect their morphology of the selected adsorbents as shown in figure 4.11.

Based on the SEM results, the corrosion and gathering of the surface are observed. The corroded surface can be indicative of the improvement in the removal efficiency because the adsorbents have larger surface area. The sodium titanate material is unstable in alkaline media, and causes a partial dissolution of the adsorbents structure.

This is interesting point of the adsorbents that have hydrothermal treatment as shown in figure 4.11 A-C; their Ni removal performance is higher even after regeneration indicating that the hydrothermal treatment at optimal condition can produce the high Ni removal performance of the adsorbents. Nevertheless, the peak of adsorption performance will probably depend on a number of usage and decreased when the surface changes.

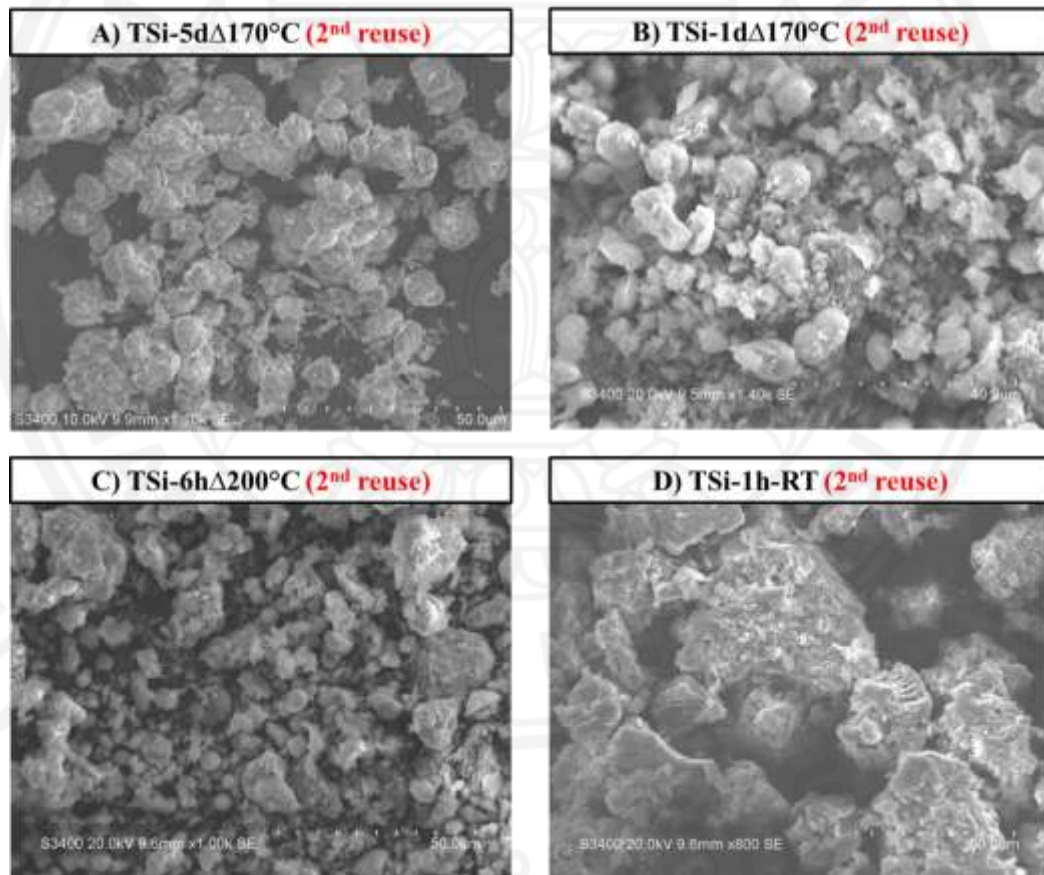


Figure 4. 11 SEM images of selected adsorbents after regeneration and reusability

#### 4.6.2.2 The functional group of the selected adsorbents

According to the Ni adsorption of the selected adsorbents after regeneration and reuse, the Ni removal efficiency of the selected adsorbents is increased. Especially TSi-6h $\Delta$ 200°C that has the highest adsorption capacity, it was significantly increased in the second and the third cycle of the Ni adsorption process. A few amount of NaOH has still remain in the selected adsorbents structure due to the hydroxyl group (OH<sup>-</sup>) from NaOH solution is exchanged with Na<sup>+</sup> and connected with Si in the structure. Therefore, the second and third cycle has the change of structure of selected adsorbents.

This discussion can be proven by FTIR as shown in figure. 4.12, the sharp bands at 725 and 624 cm<sup>-1</sup>, which is indicative of the natisite or titanosilicate, is destroyed. While the selected adsorbents were regenerated by 0.5M NaOH, that shows peak at 1630 cm<sup>-1</sup> is assigned to OH<sup>-</sup> stretching from water molecules [84] and the isopropoxide group that occur from precursor remain in structure is shown at 850 cm<sup>-1</sup> [85]. Therefore, these peaks can prove that OH<sup>-</sup> group still remains in structure. Beside the hydroxide group, the sulfate group was also remained in the structure as appear at 1118 cm<sup>-1</sup> that reveals the sulfate anions from the nickel sulfate solution [80].

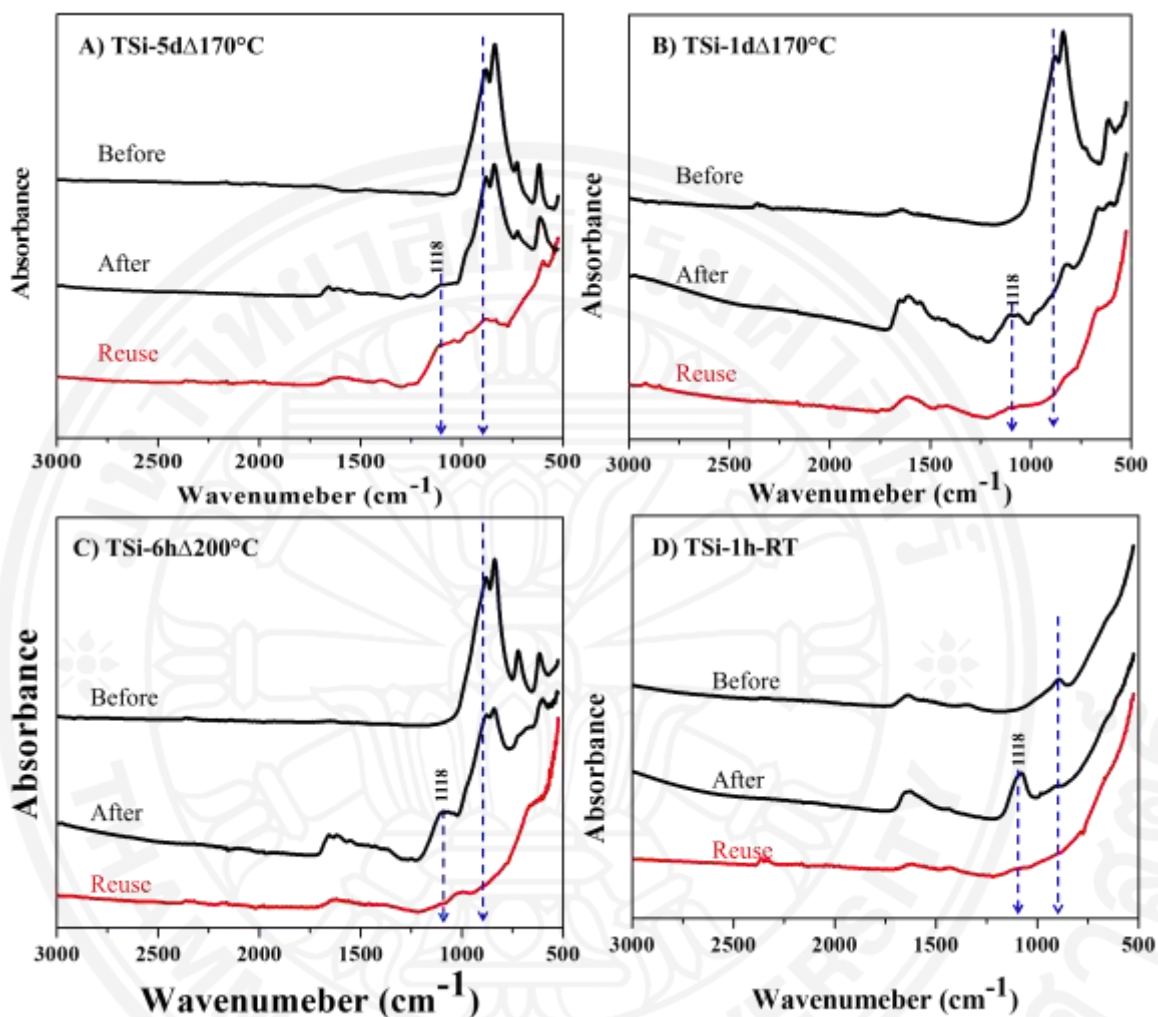


Figure 4.12 FTIR spectra of selected adsorbents after reusability

In order to compare the hydroxide group that occurs from the  $\text{Ni}(\text{OH})_2$  to that observed on the regenerated adsorbent. The  $\text{Ni}(\text{OH})_2$  on an adsorbent may occur from the adsorbed Ni on the adsorbent and the  $\text{OH}^-$  in the NaOH solution.

As seen in figure 4.13, the selected adsorbents after regeneration with 0.5M NaOH and reusability with Ni adsorption process, those are shown the decreasing of structure in both crystal and amorphous. Moreover, they are compared with the homemade of  $\text{Ni}(\text{OH})_2$  (figure 4.13E) and the  $\text{NiSO}_4$  powder (figure 4.13F). The predominant peaks of the sodium titanosilicate are damaged while reusability in second



times. Beside the destruction, the peak of  $\text{Ni}(\text{OH})_2$  is displayed at  $650\text{ cm}^{-1}$  [66], especially in TSi-6h $\Delta$ 200°C that highest adsorption capacity and TSi-1d $\Delta$ 170°C. The board peak at 600-700  $\text{cm}^{-1}$  is assigned to Ni-O stretching vibration mode [86]

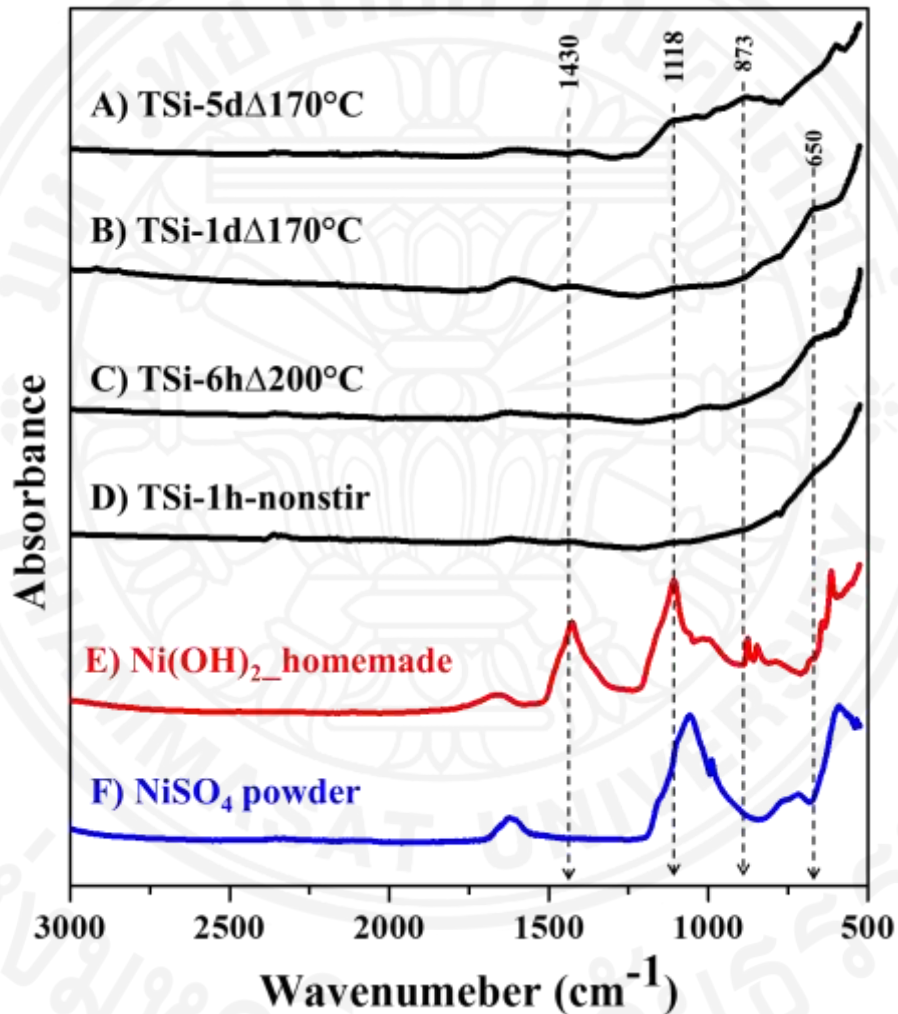


Figure 4. 13 FTIR of selected adsorbents after reusability in second cycle are compared with the homemade NiOH and the NiSO<sub>4</sub> powder.

#### 4.7 The real wastewater adsorption of the selected adsorbents

In this section, the selected adsorbents are used for Ni removal in the real wastewater from the electroplating plant. Moreover, the Ni removal efficiency of the real wastewater is compared with the synthetic Ni solution at the similar concentration.

The real wastewater is obtained from local electroplating industry which is offered for chromium and nickel plating. The real wastewater contains Ni concentration of 93.4 mg/l in the solution, which is investigated by ICP-OES. It also shows pH at 6.02. The Ni concentration in real wastewater is similar to the synthetic Ni solution at 100 mg/l.

Hence, figure 4.14 shows the comparison of the Ni removal efficiency between the real wastewater and the synthetic Ni solution at 100 mg/l. TSi-6h $\Delta$ 200°C shows the highest Ni removal efficiency in both the real wastewater and the synthetic Ni solution, that is about 84% and 99%, respectively.

According to the real wastewater, it contains mostly the mixture of the various metals. The other metals in real wastewater may be competitive with Ni in the solution to adsorb onto the surface of the selected adsorbents. For this reason, the Ni removal efficiency from the real wastewater of the selected adsorbents is slightly lower than the laboratory-made Ni solution as shown in figure 4.14.

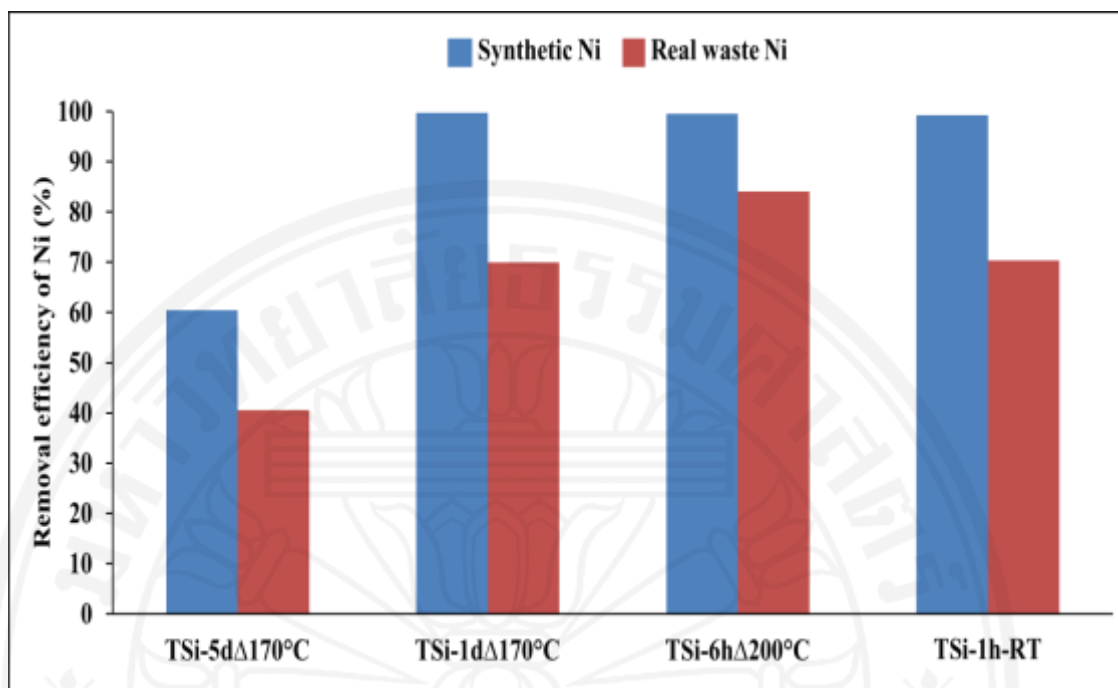


Figure 4.14 Ni removal efficiency of the selected adsorbent is compared between the real wastewater and the synthetic Ni solution

## Chapter 5

### Conclusions and Recommendation

#### 5.1 Conclusions

The main aim of this thesis was to investigate the Ni removal performance of the sodium titanate by using the adsorption and ion exchange properties. Additionally, the changed characterizations of the adsorbents affect the Ni removal performance. The sodium titanate was successfully synthesized at the various hydrothermal time and temperature such as TSi-5d $\Delta$ 170°C, TSi-1d $\Delta$ 170°C, TSi-6h $\Delta$ 170°C, TSi-6h $\Delta$ 200°C, and TSi-1h- RT.

The structure of the adsorbents is matched with the natisite pattern. The adsorbent that has not been hydrothermal reaction cannot be matched with natisite but this adsorbent shows the amorphous (TSi-1h-RT). On the other hands, the various hydrothermal time from 6 hours, 1day, and 5 days resulting in adsorbents with different crystallinity. The longest hydrothermal time of TSi-5d $\Delta$ 170°C has the highest crystallinity and then it was gradually decreased by the synthesis time. This is likely due to the short hydrothermal time that does not allow for the crystallization of the sorbent from the silicon and titanium precursors. For example, TSi-1d $\Delta$ 170°C shows XRD pattern that are less sharp and less intense compared to that of the TSi-5d $\Delta$ 170°C indicating that the crystalline phase has formed but the crystal has not fully developed. When Ni adsorption, no new phases occur in the structural adsorbents, only the peak intensity decreased. The structure results are also in accordance with the morphology results and Ni adsorption performance.

The morphology characterization studies of the adsorbents before and after Ni adsorption are shown that the surface of the longest synthesis time has the full disc-shape and clam shape and then this shape was gradually decreased by the synthesis time. Whereas the shortest synthesis time of 1 hour, the morphology was looked like irregular shape. After Ni adsorption, the morphology of all adsorbents are observed that their

morphology be similar to the shape before Ni adsorption excepting somewhat may be rounder and more packed together.

The functional group characterization of the adsorbents before and after Ni adsorption shows that the predominant peak of the titanosilicate decreased after Ni adsorption. In addition, the sulfate peak that came from nickel sulfate solution also showed in the spectra after Ni adsorption.

From the batch Ni adsorption experiment, the Ni adsorption performance of the adsorbents affected in turn with the crystalline structure. The highest Ni adsorption capacity is 108 mg Ni/g sorbent that is TSi-6h $\Delta$ 200 $^{\circ}$ C, which is fitted with the Langmuir model. Beside this adsorbent, the maximum adsorption capacity of the other selected adsorbents is 75, 89 and 101 mg Ni/g sorbent followed by TSi-5d $\Delta$ 170 $^{\circ}$ C, TSi-1h-RT, and TSi-1d $\Delta$ 170 $^{\circ}$ C, respectively. The highest crystalline structure has the lowest the Ni adsorption performance. It is probably due to the rigid crystalline structure that makes it difficult for Na<sup>+</sup> to be released out in exchange with Ni<sup>2+</sup>. Meanwhile, TSi-6h $\Delta$ 200 $^{\circ}$ C has the highest Ni adsorption performance which may be easier for Ni<sup>2+</sup> to diffuse into the structure and also for the Na<sup>+</sup> to be released.

Moreover, the Ni removal performance of the selected adsorbents from this study is higher than the commercial-grade resin that is the reason why these adsorbents are an attractive material.

Furthermore, the adsorbents after Ni adsorption are used for regeneration and reuse in second and third time. The morphology and functional group characterization are provided in order to investigate their characterization changed which is found that no IR peak of the predominant peak occurred and the surface also corroded.

In this study, the predominant mechanism of Ni adsorption on the adsorbent is the exchangeable between Na<sup>+</sup> ions and Ni<sup>2+</sup> ions. The mole ratio between the Na<sup>+</sup> and Ni<sup>2+</sup> are very close to the ideal ratio of 2 for all adsorbents due to two Na<sup>+</sup> are expected to be released from the adsorbent and one Ni<sup>2+</sup> ion for charge balance to occur.

## 5.2 Recommendation and future work

In this study, the sodium titanate has been investigated for their effectiveness in the Ni adsorption performance from real wastewater; however, the batch Ni adsorption was modeled from the laboratory-made Ni solution. The Ni adsorption performance in real wastewater is lower than the laboratory-made Ni solution owing to the competitive ions between Ni and other metal are adsorbed onto the adsorbents.

Therefore, further work may be discussed about the other metals removal, which is highly related to the wastewater problem such as metal from mining process. Moreover, an effective method to recover the precious metal from regenerant solution should be found out in further work.

## References

1. Al-Shannag, M., et al., *Heavy metal ions removal from metal plating wastewater using electrocoagulation: Kinetic study and process performance*. Chemical Engineering Journal, 2015. **260**: p. 749-756.
2. Ijadi Bajestani, M., S.M. Mousavi, and S.A. Shojaosadati, *Bioleaching of heavy metals from spent household batteries using Acidithiobacillus ferrooxidans: Statistical evaluation and optimization*. Separation and Purification Technology, 2014. **132**: p. 309-316.
3. Travis, J., T. Sutton, and W. Skroch, *A technique for determining the deposition of heavy metals in pesticides*.
4. Suthar, S., P. Sajwan, and K. Kumar, *Vermiremediation of heavy metals in wastewater sludge from paper and pulp industry using earthworm Eisenia fetida*. Ecotoxicology and Environmental Safety, 2014. **109**: p. 177-184.
5. Coman, V., B. Robotin, and P. Ilea, *Nickel recovery/removal from industrial wastes: A review*. Resources, Conservation and Recycling, 2013. **73**: p. 229-238.
6. Malkoc, E., *Ni(II) removal from aqueous solutions using cone biomass of Thuja orientalis*. Journal of Hazardous Materials, 2006. **B137**: p. 899-908.
7. Ngole, V. and G. Ekosse, *Copper, nickel and zinc contamination in soils within the precincts of mining and landfilling environments*. International Journal of Environmental Science and Technology, 2012. **9**(3): p. 485-494.
8. Almazán-Ruiz, F.J., et al., *Nickel recovery from an electroplating rinsing effluent using RCE bench scale and RCE pilot plant reactors: The influence of pH control*. Chemical Engineering Research and Design, 2015. **97**: p. 18-27.
9. Shukla, A.K., S. Venugopalan, and B. Hariprakash, *Nickel-based rechargeable batteries*. Journal of Power Sources, 2001. **100**(1-2): p. 125-148.
10. Denkhaus, E. and K. Salnikow, *Nickel essentiality, toxicity, and carcinogenicity*. Critical Reviews in Oncology/Hematology, 2002. **42**(1): p. 35-56.
11. Sun, Y., et al., *Adsorption and cosorption of ciprofloxacin and Ni(II) on activated carbon-mechanism study*. Journal of the Taiwan Institute of Chemical Engineers, 2014. **45**(2): p. 681-688.
12. Shaidan, N.H., U. Eldemerdash, and S. Awad, *Removal of Ni(II) ions from aqueous solutions using fixed-bed ion exchange column technique*. Journal of the Taiwan Institute of Chemical Engineers, 2012. **43**(1): p. 40-45.
13. Mohsen-Nia, M., P. Montazeri, and H. Modarress, *Removal of Cu<sup>2+</sup> and Ni<sup>2+</sup> from wastewater with a chelating agent and reverse osmosis processes*. Desalination, 2007. **217**(1-3): p. 276-281.
14. Ahluwalia, S.S. and D. Goyal, *Microbial and plant derived biomass for removal of heavy metals from wastewater*. Bioresource Technology, 2007. **98**(12): p. 2243-2257.
15. Kwon, T.-N. and C. Jeon, *Adsorption characteristics of sericite for nickel ions from industrial waste water*. Journal of Industrial and Engineering Chemistry, 2013. **19**(1): p. 68-72.

16. Argun, M.E., *Use of clinoptilolite for the removal of nickel ions from water: Kinetics and thermodynamics*. Journal of Hazardous Materials, 2008. **150**(3): p. 587-595.
17. Álvarez-Ayuso, E., A. García-Sánchez, and X. Querol, *Purification of metal electroplating waste waters using zeolites*. Water Research, 2003. **37**(20): p. 4855-4862.
18. Ajmal, M., et al., *Adsorption studies on Citrus reticulata (fruit peel of orange): removal and recovery of Ni(II) from electroplating wastewater*. Journal of Hazardous Materials, 2000. **79**(1-2): p. 117-131.
19. Oleksienko, O., et al., *Removal of strontium (Sr<sup>2+</sup>) from aqueous solutions with titanosilicates obtained by the sol-gel method*. Journal of Colloid and Interface Science, 2015. **438**(0): p. 159-168.
20. Kostov-Kytin, V., et al., *Hydrothermal synthesis of microporous titanosilicates*. Microporous and Mesoporous Materials, 2007. **105**(3): p. 232-238.
21. Teresia Möller \*, R.H., Jukka Lehto, *Ion exchange of <sup>85</sup>Sr, <sup>134</sup>Cs and <sup>57</sup>Co in sodium titanosilicate and the effect of crystallinity on selectivity*. Separation and Purification Technology, 2002. **28**: p. 13-23.
22. Cundy, C.S. and P.A. Cox, *The hydrothermal synthesis of zeolites: Precursors, intermediates and reaction mechanism*. Microporous and Mesoporous Materials, 2005. **82**(1-2): p. 1-78.
23. Möller, T., R. Harjula, and J. Lehto, *Ion exchange of <sup>85</sup>Sr, <sup>134</sup>Cs and <sup>57</sup>Co in sodium titanosilicate and the effect of crystallinity on selectivity*. Separation and Purification Technology, 2002. **28**(1): p. 13-23.
24. V. Kostov-Kytin, S.F., O.Petrov, *Hydrothermal Synthesis and successive transformation of paranatisite into natisite*. Comptes rendus de L'Académie bulgare des Sciences, 2002: p. 61-64.
25. Kostov-Kytin, V., et al., *Atomic arrangements in amorphous sodium titanosilicate precursor powders*. Microporous and Mesoporous Materials, 2005. **86**(1-3): p. 223-230.
26. Tripathi, A., D.G. Medvedev, and A. Clearfield, *The crystal structures of strontium exchanged sodium titanosilicates in relation to selectivity for nuclear waste treatment*. Journal of Solid State Chemistry, 2005. **178**(1): p. 253-261.
27. Nalaparaju, A., et al., *Exchange of heavy metal ions in titanosilicate Na-ETS-10 membrane from molecular dynamics simulations*. Journal of Membrane Science, 2009. **335**(1-2): p. 89-95.
28. Clearfield, A., *Structure and ion exchange properties of tunnel type titanium silicates*. Solid State Sciences, 2001. **3**(1-2): p. 103-112.
29. Registry, A.f.T.S.a.D., *TOXICOLOGICAL PROFILE FOR NICKEL* U.S.D.O.H.A.H. SERVICES, Editor. 2005, Public Health Service
30. Center, N.S.R., *Properties of Matter Element Card 14, Lesson 21, Nickel element card*
31. BV, L., *Nickel - Ni*. 2015.
32. Chiu, H., K. Tsang, and R. Lee, *Treatment of electroplating wastes*. J. Inst. Water Pollut. Control, 1987. **86**(1): p. 12-19.



33. Benvenuti, T., et al., *Recovery of nickel and water from nickel electroplating wastewater by electrodialysis*. Separation and Purification Technology, 2014. **129**: p. 106-112.
34. Jadhav, U.U. and H. Hong, *Removal of nickel and cadmium from battery waste by a chemical method using ferric sulphate*. Environmental Technology (United Kingdom), 2014. **35**(10): p. 1263-1268.
35. Al-Mansi, N.M. and N.M. Abdel Monem, *Recovery of nickel oxide from spent catalyst*. Waste Management, 2002. **22**(1): p. 85-90.
36. Cempel, M. and G. Nickel, *Nickel: a review of its sources and environmental toxicology*.
37. Department, P.C. *Standard of effluent from industrial estates*. 1996; Available from: [http://www.pcd.go.th/info\\_serv/reg\\_std\\_water04.html](http://www.pcd.go.th/info_serv/reg_std_water04.html).
38. Das, K., S. Das, and S. Dhundasi, *Nickel, its adverse health effects & oxidative stress*. Indian Journal of Medical Research, 2008. **128**(4): p. 412.
39. Prevention, C.f.D.C.a. *International Chemical Safety Cards(ICSC)*. 2014; Available from: <http://www.cdc.gov/niosh/ipcsneng/neng0062.html>.
40. (PRC), C.C.R.P.U. *CARCINOGENS, MUTAGENS, REPRODUCTIVE TOXICANTS*. 2009; Available from: <http://www.prc.cnrs-gif.fr/IMG/pdf/cmr-criteria-clp.pdf>.
41. V. Coman, B.R., P. Ilea \*, *Nickel recovery/removal from industrial wastes: A review*. Resources, Conservation and Recycling, 2013. **73**: p. 229-238.
42. Qiu, W. and Y. Zheng, *Removal of lead, copper, nickel, cobalt, and zinc from water by a cancrinite-type zeolite synthesized from fly ash*. Chemical Engineering Journal, 2009. **145**(3): p. 483-488.
43. Fu, F. and Q. Wang, *Removal of heavy metal ions from wastewaters: A review*. Journal of Environmental Management, 2011. **92**(3): p. 407-418.
44. Mavrov, V., et al., *Study of new integrated processes combining adsorption, membrane separation and flotation for heavy metal removal from wastewater*. Desalination, 2003. **157**(1-3): p. 97-104.
45. Yavuz, Ö., Y. Altunkaynak, and F. Güzel, *Removal of copper, nickel, cobalt and manganese from aqueous solution by kaolinite*. Water Research, 2003. **37**(4): p. 948-952.
46. Kandah, M.I. and J.-L. Meunier, *Removal of nickel ions from water by multi-walled carbon nanotubes*. Journal of Hazardous Materials, 2007. **146**(1-2): p. 283-288.
47. Chen, C., et al., *Adsorption behavior of multiwall carbon nanotube/iron oxide magnetic composites for Ni(II) and Sr(II)*. Journal of Hazardous Materials, 2009. **164**(2-3): p. 923-928.
48. Quintelas, C., et al., *Biosorptive performance of an Escherichia coli biofilm supported on zeolite NaY for the removal of Cr(VI), Cd(II), Fe(III) and Ni(II)*. Chemical Engineering Journal, 2009. **152**(1): p. 110-115.
49. Popuri, S.R., et al., *Adsorptive removal of copper and nickel ions from water using chitosan coated PVC beads*. Bioresource Technology, 2009. **100**(1): p. 194-199.

50. Kobya, M., et al., *Adsorption of heavy metal ions from aqueous solutions by activated carbon prepared from apricot stone*. *Bioresource Technology*, 2005. **96**(13): p. 1518-1521.
51. Malkoc, E. and Y. Nuhoglu, *Investigations of nickel(II) removal from aqueous solutions using tea factory waste*. *Journal of Hazardous Materials*, 2005. **127**(1–3): p. 120-128.
52. Zafar, M.N., R. Nadeem, and M.A. Hanif, *Biosorption of nickel from protonated rice bran*. *Journal of Hazardous Materials*, 2007. **143**(1–2): p. 478-485.
53. Chung, H.-K., et al., *Application of Langmuir and Freundlich isotherms to predict adsorbate removal efficiency or required amount of adsorbent*. *Journal of Industrial and Engineering Chemistry*, (0).
54. Liu, H., et al., *Engelhard titanasilicate-1 and Engelhard titanasilicate-2 as promising adsorbents in multivalence heavy metal removal*. *Journal of Environmental Chemical Engineering*, 2015. **3**(2): p. 1081-1087.
55. Choi, J.H., et al., *Adsorption behaviors of ETS-10 and its variant, ETAS-10 on the removal of heavy metals, Cu<sup>2+</sup>, Co<sup>2+</sup>, Mn<sup>2+</sup> and Zn<sup>2+</sup> from a waste water*. *Microporous and Mesoporous Materials*, 2006. **96**(1–3): p. 157-167.
56. Otero, M., et al., *Priority pollutants (Hg<sup>2+</sup> and Cd<sup>2+</sup>) removal from water by ETS-4 titanasilicate*. *Desalination*, 2009. **249**(2): p. 742-747.
57. Koupsi, Y. and A. Dyer, *Sorption of <sup>60</sup>Co on a synthetic titanasilicate analogue of the mineral penkvilksite-2O and antimonysilicate*. *Journal of Radioanalytical and Nuclear Chemistry*, 2001. **247**(1): p. 209-219.
58. Nyman, H., M. O'Keeffe, and J.-O. Bovin, *Sodium titanium silicate, Na<sub>2</sub>TiSiO<sub>5</sub>*. *Acta Crystallographica Section B*, 1978. **34**(3): p. 905-906.
59. Clearfield, A., et al., *Rates of Exchange of Cs<sup>+</sup> and Sr<sup>2+</sup> for Poorly Crystalline Sodium Titanium Silicate (CST) in Nuclear Waste Systems*. *Solvent Extraction and Ion Exchange*, 2012. **30**(3): p. 229-243.
60. Peng, G.-W. and H.-S. Liu, *FT-IR and XRD characterization of phase transformation of heat-treated synthetic natisite (Na<sub>2</sub>TiOSiO<sub>4</sub>) powder*. *Materials Chemistry and Physics*, 1995. **42**(4): p. 264-275.
61. Ismail, N., I.H. Abd El-Maksod, and H. Ezzat, *Synthesis and characterization of titanosilicates from white sand silica and its hydrogen uptake*. *International Journal of Hydrogen Energy*, 2010. **35**(19): p. 10359-10365.
62. Rizzo, C., et al., *Synthesis, characterization and adsorption capacities of microporous titanasilicate EMS-3*. *Microporous and Mesoporous Materials*, 2006. **90**(1–3): p. 153-161.
63. Sinha, A.K., et al., *Preparation of gold-titanosilicate catalysts for vapor-phase propylene epoxidation using H<sub>2</sub> and O<sub>2</sub>*, in *Studies in Surface Science and Catalysis*, D.E.D.V.P.G.P.A.J.J.A.M.P.R. E. Gaigneaux and G. Poncelet, Editors. 2000, Elsevier. p. 167-175.
64. Ali, I.M., E.S. Zakaria, and H.F. Aly, *Highly effective removal of <sup>22</sup>Na, <sup>134</sup>Cs and <sup>60</sup>Co from aqueous solutions by titanasilicate: a radiotracer study*. *Journal of Radioanalytical and Nuclear Chemistry*, 2010. **285**(3): p. 483-489.

65. Popa, K. and C.C. Pavel, *Radioactive wastewaters purification using titanosilicates materials: State of the art and perspectives*. Desalination, 2012. **293**(0): p. 78-86.
66. Hall, D.S., et al. *Nickel hydroxides and related materials: a review of their structures, synthesis and properties*. in *Proceedings of the Royal Society of London A: Mathematical, Physical and Engineering Sciences*. 2015. The Royal Society.
67. Silvestre-Albero, A., et al., *Desilication of TS-1 zeolite for the oxidation of bulky molecules*. Catalysis Communications, 2014. **44**(0): p. 35-39.
68. Olad, A., S. Ahmadi, and A. Rashidzadeh, *Removal of Nickel (II) from aqueous solutions with polypyrrole modified clinoptilolite: kinetic and isotherm studies*. Desalination and Water Treatment, 2013. **51**(37-39): p. 7172-7180.
69. Shahadat, M., M. Rafatullah, and T.T. Teng, *Characterization and sorption behavior of natural adsorbent for exclusion of chromium ions from industrial effluents*. Desalination and Water Treatment, 2015. **53**(5): p. 1395-1403.
70. Pornkamon Nalakarn<sup>1</sup>, R.M., Pakorn Opaprakasit<sup>3</sup>, Paiboon Sreearunothai, *SYNTHESIS AND CHARACTERIZATION OF SODIUM-TITANOSILICATE COATED MAGNETIC PARTICLES FOR REMOVAL OF CESIUM FROM CONTAMINATED WATER*, in *Pure and Applied Chemistry International Conference*. 2014. p. 611-614.
71. Aizawa, M., Y. Nosaka, and N. Fujii, *FT-IR liquid attenuated total reflection study of TiO<sub>2</sub>□SiO<sub>2</sub> sol-gel reaction*. Journal of Non-Crystalline Solids, 1991. **128**(1): p. 77-85.
72. Sprynskyy, M., et al., *Study of the selection mechanism of heavy metal (Pb<sup>2+</sup>, Cu<sup>2+</sup>, Ni<sup>2+</sup>, and Cd<sup>2+</sup>) adsorption on clinoptilolite*. Journal of Colloid and Interface Science, 2006. **304**(1): p. 21-28.
73. Chun-Wai Wong, J.P.B., Guohua Chen, Gordon McKay, *Kinetics and equilibrium studies for the removal of cadmium ions by ion exchange resin*. Journal of Environmental Chemical Engineering, 2014. **2**: p. 698-707.
74. Do, D.D., *ADSORPTION ANALYSIS: EQUILIBRIA AND KINETICS*, ed. r.T. Yang. Vol. 2. 1998: Imperial College Press.
75. Volesky, B., *SORPTION AND BIOSORPTION* Equilibrium (bio-)Sorption - Chapter 6,. 2004.
76. *LANGMUIR-ADSORPTION*. 2002.
77. Park, K.-W., H.J. Seo, and O.-Y. Kwon, *Mesoporous silica-pillared titanosilicate as catalytic support for partial oxidation of methane*. Microporous and Mesoporous Materials, 2014. **195**(0): p. 191-196.
78. Lucideon. *BET Surface Area Analysis & BJH Pore Size and Volume Analysis*. 2015; Available from: <http://www.ceram.com/testing-analysis/techniques/brunauer-emmett-teller-surface-area-analysis-barrett-joyner-halenda-pore-size-and-volume-analysis/>.
79. Ikeda, T., et al., *Crystal structure, characterization and thermal stability of NH<sub>4</sub><sup>+</sup>-exchanged -LIT-type zeolite*. Microporous and Mesoporous Materials, 2012. **163**: p. 42-50.

80. Liu, C. and Y. Li, *Synthesis and characterization of amorphous  $\alpha$ -nickel hydroxide*. Journal of Alloys and Compounds, 2009. **478**(1–2): p. 415-418.
81. Urlaub, R., U. Posset, and R. Thull, *FT-IR spectroscopic investigations on sol-gel-derived coatings from acid-modified titanium alkoxides*. Journal of Non-Crystalline Solids, 2000. **265**(3): p. 276-284.
82. Al-Maliki, F.J., *Detection of Random Laser Action from Silica Xerogel Matrices Containing Rhodamine 610 Dye and Titanium Dioxide Nanoparticles*. Advances in Materials Physics and Chemistry, 2012. **Vol.02No.03**: p. 6.
83. Kwon, Y.-G., et al., *Ambient-dried silica aerogel doped with TiO<sub>2</sub> powder for thermal insulation*. Journal of Materials Science, 2000. **35**(24): p. 6075-6079.
84. Bieniok, A. and K.D. Hammonds, *Rigid unit modes and the phase transition and structural distortions of zeolite rho*. Microporous Mesoporous Mater., 1998. **25**: p. 193-200.
85. Chen, Z., et al., *Modification of xylan in alkaline treated bleached hardwood kraft pulps as classified by attenuated total-internal-reflection (ATR) FTIR spectroscopy*. Carbohydrate Polymers, 2015. **127**(0): p. 418-426.
86. Ganachari, S.V., R. Bhat, and R. Deshpande, *Synthesis and characterization of nickel oxide nanoparticles by self-propagating low temperature combustion method*. Recent Research in Science and Technology, 2012. **4**(4).